STUDY OF CHAOTIC BEHAVIOUR AND THERMALIZATION IN SYK MODEL

By

RITABRATA BHATTACHARYA

PHYS08201305002

Harish-Chandra Research Institute, Prayagraj (Allahabad)

A thesis submitted to the

Board of Studies in Physical Sciences

In partial fulfillment of requirements

for the Degree of

DOCTOR OF PHILOSOPHY

of

HOMI BHABHA NATIONAL INSTITUTE

August, 2019

Homi Bhabha National Institute[1]

Recommendations of the Viva Voce Committee

As members of the Viva Voce Committee, we certify that we have read the dissertation prepared by Ritabrata Bhattacharya entitled " Study of Chaotic behaviour and Thermalization in SYK Model" and recommend that it may be accepted as fulfilling the thesis requirement for the award of Degree of Doctor of Philosophy.

Chairman – Prof. Ashoke Sen	Ashoke Sen	Date: 22/1/2020
Guide / Convener - Prof. Dileep Jatkar		Date: 22/1/2020
Examiner - Prof. Chethan Krisnhan		Date: 22/1/2020
Member 1- Prof. Anshuman Maharana	A Maharana	Date: 22/1/2020
Member 2- Prof. Anirban Basu	A. Basu	Date: 22/1/2020
Member 3- Prof. Prasenjit Sen	P Sen	Date: 22/1/20

Final approval and acceptance of this thesis is contingent upon the candidate's submission of the final copies of the thesis to HBNI.

I/We hereby certify that I/we have read this thesis prepared under my/our direction and recommend that it may be accepted as fulfilling the thesis requirement.

Date: 22-01-2020

Place: Prayagraj

Prof. Dileep Jatkar

Guide

[1] This page is to be included only for final submission after successful completion of viva voce.

STATEMENT BY AUTHOR

This dissertation has been submitted in partial fulfillment of requirements for an advanced degree at Homi Bhabha National Institute (HBNI) and is deposited in the Library to be made available to borrowers under rules of the HBNI.

Brief quotations from this dissertation are allowable without special permission, provided that accurate acknowledgement of source is made. Requests for permission for extended quotation from or reproduction of this manuscript in whole or in part may be granted by the Competent Authority of HBNI when in his or her judgment the proposed use of the material is in the interests of scholarship. In all other instances, however, permission must be obtained from the author.

Ritabrata Bhattacharya

Ritabrata Bhattacharya

DECLARATION

I, hereby declare that the investigation presented in the thesis has been carried out by me. The work is original and has not been submitted earlier as a whole or in part for a degree / diploma at this or any other Institution / University.

Ritabrata Bhattacharya

Ritabrata Bhattacharya

List of Publications arising from the thesis

Journal

1. "SYK model, Chaos and Conserved Charge", Ritabrata Bhattacharya, Subhroneel Chakrabarti, Dileep P. Jatkar and Arnab Kundu; *JHEP 1711* **2017** *180*

2. "Quantum Quenches and Thermalization in SYK models", Ritabrata Bhattacharya, Dileep P. Jatkar and Nilakash Sorokhaibam; *JHEP 1907* **2019** *066*

Preprint

1. "Chaotic Correlation functions with Complex Fermions", Ritabrata Bhattacharya, Dileep P. Jatkar and Arnab Kundu

Presentations at conferences and workshops:

1. *December 2017, National Strings Meet, NISER Bhubaneshwar, Orissa, India.*
   Presented **Talk** titled "SYk model, Chaos and Conserved charges".

2. *December 2018, Indian Strings Meet, IISER Thiruvananthapuram, Kerala, India .*
   Presented **Talk** titled "Chaotic Correlation functions with Complex fermions".

Ritabrata Bhattacharya
Ritabrata Bhattacharya

To my parents and friends

Acknowledgment

I would like to thank many people without whom the works of this thesis would not have been complete. Firstly I would like to thank my adviser Prof. Dileep P. Jatkar for discussions and guidance on the works included in this thesis. I would like to thank Prof. Ashoke Sen for many discussions and suggestions which contributed significantly to our work. Also discussions with him broadened my understanding of physics as a whole for which I am very grateful. I would also like to thank Prof. Anirban Basu, Prof. Anshuman Maharana and Prof. Sachidananda Nayak for discussions and comments which proved to be useful. I also thank Prof. Arnab Kundu for discussions and collaborations. Apart from the faculty members I would also like to thank my Graduate and Post Graduate colleagues for many discussions on physics and making the tenure of my PhD a memorable one. I mention here the names of my colleagues, and hope I will be excused for missing out any name who might deserve an acknowledgment for his or her contribution to expanding my knowledge in physics via discussions and collaborations. Thanks to Subhroneel Chakrabarti, Nilakash Sorokhaibam, Nilay Kundu(currently in faculty position) Biswajit Sahoo, Arpan Kar, Avirup Ghosh, Jayita Lahiri, Nirnoy Bask, Susovan Maity, Satadal Dutta, Samiran Roy, Sarif Khan, Arnab Priya Saha, Dibya Kanti Mukherjee, Aritra Gupta, Subhadeep Mandal, Mehedi Masood, Arijit Dutta, Titas Chanda. Finally I would like to thank my parents for their constant support.

Contents

Summary

For few years now there have been keen interest among theoretical high-energy physicists regarding a 0+1 dimensional model of Majorana fermions with random all to all interaction known as the Sachdev Ye Kitaev model or the SYK model for short. Although in condensed matter theory there have been much studies regarding thermalization and other thermodynamic properties in models without a spin glass transition for example the original Sachdev Ye (SY) model or (a simpler but of similar properties) the SYK model itself, the property which has been of most interest to people in the high energy community is that this model or more precisely, this class of models exhibit maximal chaotic behavior in the Infra Red(IR) regime or low frequency regime. This makes it interesting because as we know that the maximal chaotic behavior is exhibited by the fastest scrambler of information in nature i.e. Black Holes. So this model can potentially describe or atleast serve as a prototype for the dual of black holes.

In this thesis we look closely into the chaotic behavior of the SYK model with complex fermions in the presence of a chemical potential. In particular we look at the four point and six point OTOC. The findings of the works related to this can be nicely summarized as follows,

- We observe that the effect of the chemical potential appears through an effective coupling which is a function of both the disorder averaged coupling strength as well as the chemical potential. The maximal Lyapunov exponent becomes a sensitive function of the chemical potential via the effective coupling.
- This feature is fairly robust and holds even when we have multiple flavors of fermions in the system.
- We compute the six point OTOC numerically and plot it to extract the chaos exponent by fitting with a suitable function. The maximal chaos exponent in this case in the IR is $\approx \frac{3\pi}{\beta}$ within the numerical errors.

We also look at the SYK model with Majorana fermions when the system undergoes a quench. Our main goal is to study the thermalization of the system post the quench scenarios numerically. For this purpose we consider 2, 4, 6 and 8 point interactions where more than one type of vertex are allowed. We look at two different quench protocols namely “STEP" and “BUMP" quenches.

The main technical results of this analysis are as follows:

- In $q = 2$ theory, the two point functions do not thermalize in any of the quench scenario. But an interesting observation is that the two point functions equilibrate instantaneously as soon as both the time arguments are outside the quench region.
- In $q = 4$ theory, the two point functions thermalize for all the quench scenario. $G^{>}(t_1, t_2)$ converges exponentially towards its equilibrium expectation value. This exponential behaviour is observed as soon as both the time arguments are outside the quench region.
- In $q = 4$ theory, we also identify two exponents, of which, one is equal to the coupling and the other is proportional to the final temperature. The first one is the exponent of $G^{>}(t - t_a, t)$ as a function of t with t_a fixed, while the other is the exponent of $G^{>}(t, t_b)$ as a function of t with t_b fixed.

List of Figures

List of Tables

Introduction

The study of chaos in quantum dynamical systems has been interesting to the physics community for quite some time [1–5]. One of the key features of this phenomena is that there is no unique definition of chaos in quantum mechanics as opposed to classical mechanics. In a classical dynamical system chaos is characterized by the response of classical trajectories subjected to the initial condition. To elaborate let us denote by $q(t)$ the position of a particle at time t in a classical dynamical system, subjected to the initial condition (or position) $q(0)$. Now if we start with some different initial condition say, $q(0) + \delta q(0)$ such that the final position of the particle becomes $q(t) + \delta q(t)$, then we say that the system is chaotic if,

$$\frac{\delta q(t)}{\delta q(0)} \sim e^{\lambda_L t}. \tag{0.0.1}$$

Note that a system can be bounded yet be chaotic. The exponent λ_L is called the Lyapunov exponent and is the measure of chaos in a system. Chaos in a system can subsequently lead to ergodicity, thermalization and other coarse grained properties of the system. In quantum mechanics since trajectories of particles are ill defined, such a description is not very useful and hence there have been various descriptions of chaotic behavior in quantum mechanical systems such as the Random Matrix models [6–10], behavior of the four point Out of Time Ordered Correlation functions (OTOC) [11–14].

It was shown [11, 15, 16], following the OTOC description of chaos in a quantum systems, that Black Holes being the fastest scramblers of information in nature puts an upper bound on the value of the Lyapunov exponent and they themselves saturate this bound,

$$\lambda_L \leq \frac{2\pi}{\beta} \, . \tag{0.0.2}$$

This feature is famously known in the literature as the maximal chaotic behavior. It is for this reason that any quantum mechanical model which exhibits this phenomena is interesting to study as a dual to a geometry with Black Holes [17–20].

The Sachdev-Ye-Kitaev(SYK) model provides us with such an example. This is a 0+1 dimensional quantum mechanical model consisting of N Majorana fermions which interact among themselves. The Hamiltonian of this model is given by,

$$H = \sum_{i_1 \ldots i_q} J_{i_1 \ldots i_q} \psi^{i_1} \ldots . \psi^{i_q} \, . \tag{0.0.3}$$

Where $J_{i_1 \ldots i_q}$ is a Gaussian random distributed coupling for the q point interaction vertex. In the IR limit i.e the low energy or equivalently the strong coupling limit this model

exhibits an emergent conformal or reparametrization invariance. We work in the large N limit where only the melonic diagrams contribute to the two point function to order $\sim 1/N$. As for the four point function, the contribution to order $\sim 1/N$ for the fully connected piece comes from the ladder diagrams. One can calculate the four point OTOC at finite temperature and it exhibits a behavior as,

$$\langle \psi_i(t)\psi_j(0)\psi_i(t)\psi_j(0)\rangle \sim 1 - e^{\frac{2\pi}{\beta}t}\,, \tag{0.0.4}$$

which implies that the Lyapunov exponent saturates the bound [21].

$$\lambda_L = \frac{2\pi}{\beta}\,. \tag{0.0.5}$$

The study of chaotic behavior of quantum systems is interesting for other reasons as well, since it is widely believed that chaos leads to ergodicity and thermalization. The nature of the maximally chaotic mode and its response to perturbations of the hamiltonian by relevant operators have been one the major interest of the SYK programme also [22].

There are several generalizations of this model preserving these remarkable features. These are two-dimensional versions of the model, formulated both on the lattice [23] and in the continuum [24], models having flavor symmetry [25] and supersymmetry [26, 27]. There are also tensor models with non-random coupling sharing many properties of the SYK [28–35]. Our focus is mostly on the SYK model with complex fermions. It has been studied in from a thermodynamical perspective [36] to compute transport coefficients of a strange metal. The class of models sharing these similar features, constitute a vast areana for studying dynamical quantum phase transitions [37]. There are several other features of the SYK like models (in particular Tensor models) which have picked up interests recently, for example the finite N results i.e. non-perturbative in N [38].

For classical dynamical systems, characterized by phase space coordinates $\{q(t), p(t)\}$, where $q(t)$ and $p(t)$ are generalized positions and generalized momenta. A particular trajectory is represented by $q(t)$. High sensitivity of the late time trajectory with respect to the initial condition can be quantified as:

$$\exp\left(\lambda_{\rm L} t\right) = \frac{\partial q(t)}{\partial q(0)} \equiv \{q(t), p(t)\}\,, \tag{0.0.6}$$

where $\lambda_{\rm L}$ is the so-called Lyapunov exponent and the right-most expression above is the Poisson bracket [39]. By virtue of the correspondence principle, we obtain a quantum mechanical characterization, by replacing the Poisson bracket with a commutator: $\{q(t), p(t)\} \rightarrow -i\hbar[q(t), p(t)]$ [16]. Instead of computing the commutator, one calculates the squared commutator, so that there is no spurious cancellation due to destructive phases. This argument, however, is limited and does not necessarily imply that allowing for such phases will always cancel the chaotic growth. In this article, we will calculate the cubic power of the commutator, which will explicitly display the exponential growth behaviour.

Thus, we can define a generic function for the diagnostic of chaos:

$$C_{(n)}(t_1, t_2) \equiv \langle [V(t_1), W(t_2)]^n \rangle\,, \tag{0.0.7}$$

where $n \in \mathbb{Z}_+$, and V and W are two self-adjoint operators and the expectation value is defined with respect to a particular state of the system. Note that, in defining the chaos diagnostic in (0.0.7), we have recast the chaotic property as a feature of n-point correlation function of the system. A straightforward analogy with the classical limit does not preclude a two-point function from displaying the exponential growth, but we know of no explicit example of the same. In this article, we will explicitly discuss the case for $n = 3$ in a thermal state.

Before doing so, let us briefly look at the $n = 2$ case. Written explicitly, the commutator contains various four-point functions with no particular time-ordering, since t_1 and t_2 are defined without any ordering. For a thermal state expectation value, using the KMS conditions[1], it is further possible to rearrange the various four-point functions in terms of two pieces: one time-ordered four-point function and another out-of-time-ordered correlator (OTOC). These are given by $\langle V(0)V(0)W(t)W(t)\rangle$ and $\langle V(0)W(t)V(0)W(t)\rangle$, respectively, choosing $t_1 = 0$ and $t_2 = t$. The time-ordered correlator does not display the exponential growth, it is contained in the four-point OTOC. There have been exhaustive studies of OTOC in quantum systems [40–42].

For $n = 3$, upon using the KMS condition, the chaos diagnostic in (0.0.7) has one time-ordered and two OTOC pieces. These are simply, $\langle V(0)V(0)V(0)W(t)W(t)W(t)\rangle$ (time-ordered) and

$$\langle V(0)W(t)V(0)W(t)V(0)W(t)\rangle, \quad \langle V(0)W(t)V(0)V(0)W(t)W(t)\rangle, \quad \langle W(t)V(0)V(0)W(t)V(0)W(t)\rangle\,, \tag{0.0.9}$$

etc, which are OTOC. While a complete understanding of the behaviour of (0.0.7) for arbitrary n is desirable, we will explore an exact calculation for $n = 3$ in this article, with a particularly simple model.

Thermalization of a system can be labeled as the non-equilibrium dynamics of the system before reaching to a final temperature. The equilibrium analytic results for many quantities fail to hold out of equilibrium for obvious reasons and hence in many cases one has to resort to numerical techniques to compute relevant quantities and study their behavior. In contemporary literature [20, 43–45] the thermalization in SYK model was studied in the presence of quantum quenches. By this we mean that assuming a system to be at equilibrium one introduces a quench (localized at $t = 0$ say) and then the dynamics of the system is studied post quench where at late times the system equilibriates to some other temperature.

Certain aspects of quantum quenches in SYK models have been studied in [43]. In this paper, using similar numerical techniques, we will study quantum quenches in $q = 2, 4$, and higher SYK models. We will consider one particular observable which is the greater

[1] KMS condition is simply the Euclidean periodicity condition on thermal correlators. For example, for two operators $V(0)$ and $W(t)$, the KMS condition on the two-point function reads:

$$\mathrm{tr}\left(e^{-\beta H}W(t)V(0)\right) = \mathrm{tr}\left(e^{-\beta H}V(0)W(t+i\beta)\right)\,. \tag{0.0.8}$$

Here β is the inverse temperature. Evidently, this condition can be used to interchange the order of the operators inside a thermal correlator.

Green's function $G^{>}(t_1, t_2)$,

$$G^{>}(t_1, t_2) = -i \sum_{i=1}^{N} \langle \psi_i(t_2)\psi_i(t_1)\rangle \ . \tag{0.0.10}$$

For majorana fermions, all other two-point functions can be calculated from $G^{>}(t_1, t_2)$. The non-trivial time evolution of $G^{>}(t_1, t_2)$ can be examined by exactly solving its equations of motion which are the Kadanoff-Baym(KB) equations. Our analysis will involve changing various parameters with two different kinds of time dependence. The usual quench protocol in condensed-matter literature is changing, suddenly[2] or smoothly but rapidly, the parameters from one value to another different value. We will consider sudden change from one value to another, which we call step quench. In addition to this, we will also study bump quench, in which the coupling changes for a finite time interval before returning back to the original value[3]. We follow the convention $q = k$ quench when the final hamiltonian of the system has k fermion interaction and the couplings J_q undergo quench with $q \neq k$. We will also consider only sudden limit for both step and bump quenches.

This thesis contains a study of chaos and thermalization in SYK models. To be a bit more precise, we study the chaotic behavior and the six point correlation function of the SYK model with complex fermions with a chemical potential corresponding the conserved $U(1)$ charge, $\sum_i \psi_i^\dagger \psi_i$ for the complex fermions.
We first look at how the maximally chaotic behavior is affected by the introduction of the chemical potential. To be able to get an analytic handle on the computations we work in the regime of large q, i.e. $q \to \infty$. We find that in this limit the response of the maximal Lyapunov exponent against μ can be determined through an effective coupling.
Then we look at the non conformal part of six point function of the fermions and try to see both the triple short time limit and the OTOC and how they vary with μ (the chemical potential). We use the numerical methods to calculate the six point function because the analytic computation of the six point function is hard and not tractable. Instead the numerical results help us deduce the behavior of the six point function for various parametric values.
Lastly we look at the thermalization in SYK model (with Majorana) with different quench protocols, the so called "STEP" and "BUMP" quenches. We determine the behavior of the two point function as a function of time by numerically evolving the Kadanoff-Baym equations.
The organization of the thesis is as followed,

- In Chapter 1 we briefly review the SYK model with complex fermions for setting up the notations and some background. We give the main and relevant results and indications on how to derive the important formulas.
- Chapter 2 contains the works on the behavior of the maximal Lyapunov exponent λ_L when we turn on a chemical potential. Here we derive in details all the relevant

[2] The smallest scale in the sudden limit is the time scale over which the couplings change.
[3] Although bump quenches are not well studied in condensed-matter literature, they are more relevant to black hole physics (using AdS/CFT) than step quenches [46, 47].

quantities and conclude with a generalization of this phenomena to multiple flavors of fermions.

- In Chapter 3 we take a look at computing the six point function of complex fermions and focusing on the non conformal piece. We look at the chaotic behavior of this piece of the six point function by analyzing the the OTO configuration. We also look at the behavior as we take the triple short time limit for the six point function. The works of Gross and Rosenhaus [48, 49] were followed in this regard.

- Lastly in Chapter 4 we present the work on thermalization of the SYK model in two different quench scenarios, "STEP" and "BUMP". We also compute exponents which characterize the thermalization process out of equilibrium and determine them as a function of the coupling or as a function of the effective temperature.

- We devote Chapter 5 to the conclusions and discussions for all the works.

All the chapters contain their own appendices.

1 SYK model with complex fermions and chemical potential

The model we consider is a simple generalization of the so-called Sachdev-Ye-Kitaev (SYK) system [21, 50–52], in which one considers fermionic degrees of freedom with an all-to-all interaction. The interaction coupling is drawn from a random Gaussian distribution with a zero mean value and a given standard deviation characterizing the width. In the large N limit, in which the number of fermionic degrees of freedom becomes infinite, the system becomes analytically tractable in the sense that the corresponding Schwinger-Dyson equations can be explicitly determined. The solution of this equation readily determines the two-point function, as a function of the coupling strength, in general. In particular, in the low energy limit, this Schwinger-Dyson equation is analytically solvable and yields a two-point function with a manifest $SL(2, R)$ symmetry. In the infra-red (IR), this is described by a conformal field theory (CFT), and the two-point function breaks the conformal group into the $SL(2, R)$ subgroup. In the large N limit, further, the four-point correlator can be explicitly calculated, which yields the corresponding Lyapunov exponent: $\lambda_L = 2\pi T$, where T is the temperature of the thermal state. Here, we are working in natural units. This Lyapunov exponent saturates the so-called chaos bound [11]. Intriguingly, the chaos bound saturation also occurs for black holes, in which the local boost factor at the event horizon determines the corresponding Lyapunov exponent as well as the corresponding Hawking temperature. Only extremal black holes have an $SL(2, R)$ global symmetry, due to the existence of an AdS_2 sector near the horizon. Correspondingly, the low energy conformal system coming from the SYK model can be shown to capture the essential physics of the AdS_2 [53].

This theory is supposed to have a holographic dual [18, 46, 51, 52, 54–56]. Since SYK is a (nearly) CFT1, it is naturally assumed to be dual to (nearly) AdS_2 geometry. Indeed, at low temperatures the effective action of the model is given by a Schwarzian derivative , which also appears in dilaton gravity in AdS_2 [57–59]. However, full knowledge of a gravity dual of the SYK model is still not known.

In addition to pseudo-Goldstone mode of the original SYK, or h = 2 mode of [6], the complex SYK model contains a mode associated with U(1) charge. Since the U(1) charge is conserved, the corresponding mode has the dimension h = 0. In the real SYK model, the four-point function is a sum over eigenfunctions with integer h, including the h = 2 mode. But since it corresponds to an existing operator in the spectrum, it makes the four-

point function to diverge. The same mode also contributes to the Lyapunov exponent of the out of time order correlators. One might expect that the h = 0 mode in the complex SYK also causes divergence in the four-point function and exhibit chaotic behaviour.

1.1 The SYK model

We will begin by briefly recalling the SYK model. The SYK model is describes all-to-all random interactions between N Majorana fermions in (0 + 1) dimension involving q fermions at a time. The Hamiltonian is given by [21, 50]

$$H = (i)^{q/2} \sum_{1\leq i_1\leq \ldots\ldots i_q\leq N} j_{i_1\ldots i_q}\psi_{i_1}\ldots\psi_{i_q}\,, \tag{1.1.1}$$

where $q \leq N$ and q = even. The set of couplings $\left\{j_{i_1\ldots i_q}\right\}$ are drawn from a random distribution, such as a Gaussian one, described by

$$\mathcal{P}\left(j_{i_1\ldots i_q}\right) = \exp\left[-\frac{N^3 j^2_{i_1\ldots i_q}}{12J^2}\right]\,, \tag{1.1.2}$$

where $\mathcal{P}$ denotes the probability distribution. The gaussian distribution for a random variable means the average value of the couplings $j_{i_1\ldots i_q}$ is zero and the two point average with all indices contracted is non-vanishing,

$$\left\langle j_{i_1\ldots i_q}\right\rangle = 0\,, \quad \left\langle j^2_{i_1\ldots i_q}\right\rangle = \frac{J^2\,(q-1)!}{N^{q-1}}\,. \tag{1.1.3}$$

The Majorana condition on the fermions simply means that they satisfy the anti-commutation relation,

$$\left\{\psi_i, \psi_j\right\} = \delta_{ij}\,. \tag{1.1.4}$$

The Lagrangian corresponding to (1.1.1) is given by

$$S = \int d\tau L_{\rm E}\left(\{\psi_i\}, \left\{\frac{d\psi_i}{d\tau}\right\}\right)\,, \quad L_{\rm E} = \frac{1}{2}\psi_i\frac{d\psi_i}{d\tau} - H\,, \tag{1.1.5}$$

$$\text{equivalently} \quad L = -\frac{1}{2}\psi_i\frac{d\psi_i}{dt} - H\,, \quad \text{with} \quad t = -i\tau\,. \tag{1.1.6}$$

In the above $L_{\rm E}$ and L corresponds to the Lagrangian in Euclidean and Minkowski signatures, respectively.

To compute correlators at finite temperature the Schwinger-Keldysh formalism is employed in which, the observables are computed by integrating along the closed-time contour C. The initial state is evolved along this contour both forward and backwards in time. The contour-ordered Green 's function is defined as [43],

$$iG(t_1, t_2) = \langle T_C\left(\psi_i(t_1)\psi_i(t_2)\right)\rangle = \theta_C(t_1 - t_2)\langle\psi_i(t_1)\psi_i(t_2)\rangle - \theta_C(t_2 - t_1)\langle\psi_i(t_2)\psi_i(t_1)\rangle\,. \tag{1.1.7}$$

The correlation function in the path integral formalism is computed by inserting the components of fields on the forward and return path of the contour. The components of the matrix Green's functions that we will be interested in are called greater (lesser) Green's functions, denoted as $G^{>(<)}(t_1, t_2)$, and are defined in the following manner [1]

$$\begin{aligned} G^{>}(t_1, t_2) &\equiv G(t_1^-, t_2^+) = -i\langle\psi_i(t_2)\psi_i(t_1)\rangle \,, \\ G^{<}(t_1, t_2) &\equiv G(t_1^+, t_2^-) = i\langle\psi_i(t_1)\psi_i(t_2)\rangle \,, \end{aligned} \tag{1.1.8}$$

where by t_i^+ we mean t_i on the upper contour and t_i^- denotes t_i on the lower contour, and the contracted index i simply denotes a sum over i. The relative minus sign above is due to swapping of the position of two Majorana fermions under contour ordering. From the above definitions, for Majorana fermions,

$$G^{<}(t_2, t_1) = -G^{>}(t_1, t_2) \,. \tag{1.1.9}$$

This relation holds even for non-equilibrium dynamics [43, 60].

This model exhibits conformal symmetry in the infrared which is spontaneously broken by the $h = 2$ mode, where h is the quantum number of the $SL(2)$ subgroup of the conformal symmetry. This $h = 2$ mode has chaotic behaviour for $q \geq 4$. It turns out that the $h = 2$ mode saturates the chaos bound $\lambda_L = 2\pi/\beta$ [11]. The model with only $q = 2$ term, however, does not have chaotic behaviour. This is clearly due to the quadratic nature of the action and as a result the model is integrable.

1.1.1 SYK model with Complex Fermions

In order to introduce a chemical potential, we will explore the model involving complex fermions. This model has been studied earlier in the condensed matter context [36], focussing on transport properties and thermodynamics; and in the context of chaos in [61]. We are interested in the large q expansion of the complex fermion model with an addition of a non-vanishing chemical potential, which seems analogous to adding a mass term.

The Hamiltonian for the SYK model with complex fermions is

$$H = \sum J_{i_1 i_2 \ldots i_{q/2} i_{q/2+1} \ldots i_q} \psi^\dagger_{i_1} \psi^\dagger_{i_2} \ldots \psi^\dagger_{i_{q/2}} \psi_{i_{q/2+1}} \ldots \psi_{i_q} \,. \tag{1.1.10}$$

In what follows we will use the notations and conventions used in [36]. In addition to this interaction term we introduce a chemical potential μ. We are interested in studying the effect of a conserved charge on the chaotic behaviour of the model. Some of the earlier works [36, 61] have analysed this model with either quartic interactions or in the non-chaotic regime. We will work in the large q limit and find out how the Lyapunov exponent changes as we tune in the chemical potential.

To establish this fact we need to first collect all the necessary ingredients for explaining this behavior. An exhaustive study of this model is done in [61], we will mention some of the essential features that will be necessary for our analysis. In addition to the higher dimensional operators of the form $O_n = \frac{1}{N}\sum_i \psi_i^\dagger \partial_t^{2n+1} \psi_i$ which behave in a manner similar to

[1] We use the commutation relation $\left\{\psi_i, \psi_j\right\} = \delta_{ij}$. So, $G^{>}(t, t) = -i/2$ and $G^{<}(t, t) = i/2$.

those found in the SYK model with Majorana fermions; we also have the operators of the form $\tilde{\mathcal{O}}_n = \frac{1}{N}\sum_i \psi_i^\dagger \partial_t^{2n}\psi_i$. The lowest lying mode of these operators give the Schwarzian mode and the $U(1)$ charge respectively. In absence of a mass like term in the action the two point function of the particle and anti-particle are the same in the free case as well as the low energy limit of the interacting theory.

$$G_{free}(\tau) = \frac{1}{2}\text{sgn}(\tau), \quad G_c(\tau) = b\frac{\text{sgn}(\tau)}{|\tau|^{\frac{2}{q}}}\,, \tag{1.1.11}$$

where, $G_c(\tau)$ is the propagator in the conformal limit. In the low energy, *i.e.*, IR limit it is possible to obtain the four point function of the fermions using the expansion in the eigen-basis of the quadratic Casimir operator.

The conformal Casimir operator in terms of the cross ratio χ is given by,

$$C(\chi) = \chi^2(1-\chi)\partial_\chi^2 - \chi^2\partial_\chi\,. \tag{1.1.12}$$

This is easy to check since, $L_0^{(\tau)} = -\tau\partial_\tau - \Delta$, $L_{-1}^{(\tau)} = -\partial_\tau$ and $L_1^{(\tau)} = -\tau^2\partial_\tau - 2\Delta\tau$ we have the Casimir as,

$$\begin{aligned} C_{1+2} &= (L_0^{(\tau_1)} + L_0^{(\tau_2)})^2 - \frac{1}{2}(L_1^{(\tau_1)} + L_1^{(\tau_2)})(L_{-1}^{(\tau_1)} + L_{-1}^{(\tau_2)}) - \frac{1}{2}(L_{-1}^{(\tau_1)} + L_{-1}^{(\tau_2)})(L_1^{(\tau_1)} + L_1^{(\tau_2)})\,, \\ \text{i.e.,}\quad C_{1+2} &= 2(\Delta^2 - \Delta) + 2L_0^{(\tau_1)}L_0^{(\tau_2)} - L_1^{(\tau_1)}L_{-1}^{(\tau_2)} - L_{-1}^{(\tau_1)}L_1^{(\tau_2)}\,. \end{aligned} \tag{1.1.13}$$

1.1.2 The four-point kernel and the Casimir

The eigenfunctions of the conformal Casimir also forms a eigen basis for the four point kernel in the IR limit. The eigenvalue equation of the Casimir is given by,

$$C_{1+2}\left\langle\psi^\dagger(\tau_1)\psi(\tau_2)V_h(\tau_0)\right\rangle = h(h-1)\left\langle\psi^\dagger(\tau_1)\psi(\tau_2)V_h(\tau_0)\right\rangle\,. \tag{1.1.14}$$

Where,

$$\left\langle\psi^\dagger(\tau_1)\psi(\tau_2)V_h(\tau_0)\right\rangle = f_h^A + if_h^S = \frac{\text{sgn}(\tau_1-\tau_2) + i\,\text{sgn}(\tau_1-\tau_0)\text{sgn}(\tau_2-\tau_0)}{|\tau_1-\tau_2|^{2\Delta-h}\,|\tau_1-\tau_0|^h\,|\tau_2-\tau_0|^h}\,. \tag{1.1.15}$$

When we have $V_h = 1$ or $V_h = \psi^\dagger\psi$ we get respectively an antisymmetric and a symmetric three point function,

$$\left\langle\psi^\dagger(\tau_1)\psi(\tau_2)\,1\right\rangle = \frac{\text{sgn}(\tau_1-\tau_2)}{|\tau_1-\tau_2|^{2\Delta}}\,, \tag{1.1.16}$$

$$\left\langle\psi^\dagger(\tau_1)\psi(\tau_2)\psi^\dagger\psi(\tau_0)\right\rangle = \frac{\text{sgn}(\tau_1-\tau_0)\text{sgn}(\tau_2-\tau_0)}{|\tau_1-\tau_2|^{2\Delta}}\,. \tag{1.1.17}$$

We can write

$$C_{1+2}\mathcal{F}(\tau_1,\tau_2,\tau_3,\tau_4) = C(\chi)\mathcal{F}(\chi), \quad \text{and} \quad C(\chi)F_h(\chi) = h(h-1)F_h(\chi)\,, \tag{1.1.18}$$

where

$$F_h(\chi) = \frac{\Gamma^2(h)}{\Gamma(2h)}\, {}_2F_1(h,h,2h;\chi)\ . \tag{1.1.19}$$

The eigenvalue of the Casimir operator are chosen to be real so that it is guarantied to be a hermitian operator. This implies that $h(h-1)\,\epsilon\,\mathbb{R}$ and thus we are left with,

$$h = \frac{1}{2} + i\,s\ , \quad \text{or} \quad h\,\epsilon\,\mathbb{R} \tag{1.1.20}$$

Since we have complex fermions, *i.e.*, $\psi_i = \xi_i + \mathbf{i}\eta_i$ in case of the correlation functions we have contribution of two different kinds,

$$\langle\psi^\dagger(t_1)\psi(t_2)...\rangle = \langle(\xi(t_1)\xi(t_2)+\eta(t_1)\eta_(t_2))...\rangle + \mathbf{i}\langle(\xi(t_1)\eta_(t_2)-\eta(t_1)\xi(t_2))...\rangle\ . \tag{1.1.21}$$

While the first piece, namely, the real part is anti-symmetric under the exchange of t_1 and t_2, the second piece is symmetric.

In case of the four point function if we consider the time reversal invariant contribution this leads to two different contributions namely $F^A(\tau_1,\tau_2,\tau_3,\tau_4)$ and $F^S(\tau_1,\tau_2,\tau_3,\tau_4)$ which are respectively anti-symmetric and symmetric under $t_1 \leftrightarrow t_2$ and $t_3 \leftrightarrow t_4$. The first term *i.e.*, $F^A(\tau_1,\tau_2,\tau_3,\tau_4)$ is identical to the SYK with Majorana but the second term is new and occurs in the complex fermion model. From [61] we have,

$$\begin{aligned}
\frac{F^A(\tau_1,\tau_2,\tau_3,\tau_4)}{G(\tau_{12})G(\tau_{34})} &= \alpha_0\int_0^\infty \frac{sds}{\pi^2}\frac{k^A(\frac{1}{2}+is)}{\coth(\pi s)(1-k^A(\frac{1}{2}+is))}\Psi^A_{\frac{1}{2}+is}(\chi) \\
&\quad +\alpha_0\sum_{2j>0}\frac{2j-\frac{1}{2}}{\pi^2}\frac{k^A(2j)}{1-k^A(2j)}\Psi^A_{2j}(\chi), \qquad (1.1.22)\\
\frac{F^S(\tau_1,\tau_2,\tau_3,\tau_4)}{G(\tau_{12})G(\tau_{34})} &= \alpha_0\int_0^\infty \frac{sds}{\pi^2}\frac{k^S(\frac{1}{2}+is)}{\coth(\pi s)(1-k^S(\frac{1}{2}+is))}\Psi^S_{\frac{1}{2}+is}(\chi) \\
&\quad +\alpha_0\sum_{2j+1>0}\frac{2j+\frac{1}{2}}{\pi^2}\frac{k^S(2j+1)}{1-k^S(2j+1)}\Psi^S_{2j+1}(\chi)\ , \qquad (1.1.23)
\end{aligned}$$

where

$$\chi = \frac{\tau_{12}\tau_{34}}{\tau_{13}\tau_{24}}\ , \tag{1.1.24}$$

is the conformal cross ratio and Ψ^A and Ψ^S are linear combinations of the eigen-functions of the quadratic Casimir. They are antisymmetric, respectively symmetric under the transformation,

$$\chi \to \frac{\chi}{\chi-1}\ , \tag{1.1.25}$$

which effectively exchanges the first two or last two arguments of four point function. Finally k^A and k^S are eigenvalues of the four point kernels (for antisymmetric and symmetric) which commute with the Casimir.

The next step is to deform the integration contour an take it to infinity. In this process we pick up the contributions i.e. residues of the integrand at the values of h such that $1 - k^{A,S}(h, \Delta)$ vanishes so the poles that are picked out are precisely the points where the eigenvalue of the kernel becomes unity. Here also we find a contribution from $h = 2$ for k^A. In a similar fashion one is able to deform the contour and pick the contributions such that $k^S(h, \Delta) = 1$. The values of h which satisfy these conditions approach

$$h^A = h_n = 2n + 1 + 2\Delta + O\left(\frac{1}{n}\right), \qquad n \epsilon \mathbb{Z}_+ \tag{1.1.26}$$

$$h^S = h_n = 2n + 2\Delta + O\left(\frac{1}{n}\right), \qquad n \epsilon \mathbb{Z}_+ \tag{1.1.27}$$

for large valus of n.

1.1.3 Fermion propagator, with a chemical potential

We define, following [36], the Green's function to be: $G(\tau) = -\left\langle \mathrm{T}\left(\psi(\tau)\psi^\dagger(0)\right)\right\rangle$, where the symbol T stands for time-ordering and τ is the imaginary time. The free fermion propagator, in the Fourier space, takes the form:

$$G(\mu, \omega) = \frac{1}{i\omega + \mu}\,, \tag{1.1.28}$$

which, in the real space, corresponds to the operator $(-\partial_t + \mu)$. The two point function in the interacting theory, in the large q limit, can be expanded as:

$$G(\mu, \tau) = G_0(\mu, \tau)\left(1 + \frac{g(\mu, \tau)}{q} + ..\right)\,, \tag{1.1.29}$$

where $G_0(\mu, \tau)$ is the Fourier transform of the free propagator, which at zero temperature it is given by,

$$G_0(\mu, \tau) = -e^{\mu\tau}\frac{\mathrm{sgn}(\tau)}{2}\,. \tag{1.1.30}$$

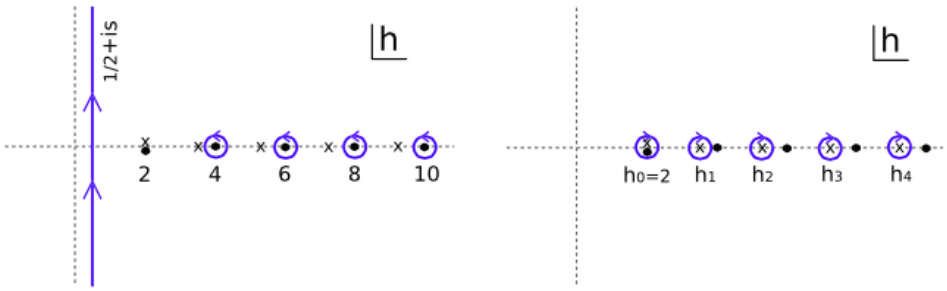

Figure 1.1: Before the deformation poles are at $h\epsilon\mathbb{Z}$ and after deformation h is such that $k^A(h, \Delta) = 1$. Figure adopted from [21]

Here Θ is the Heaviside step function. At non-vanishing temperature, however, it is obtained by evaluating the sum over Matsubara frequencies that appear in the propagator, $(i\omega_n + \mu)^{-1}$, which yields,

$$G_0(\mu,\tau) = -\frac{e^{\mu\tau}}{e^{\mu\beta}+1}, 0 \le \tau \le \beta , \tag{1.1.31}$$

$$G_0(\mu,\tau) = \frac{e^{\mu\tau}}{e^{-\mu\beta}+1}, -\beta \le \tau \le 0 . \tag{1.1.32}$$

The propagator for $\tau < 0$ is obtained using the periodicity $\tau \to \tau + \beta$. The relative sign between $\tau < 0$ and $\tau > 0$ is a reflection of the fact that $G_0(\mu,\tau)$ is a fermion propagator. Finally, the function $g(\mu,\tau)$ is the correction due to melonic diagrams to the free propagator, in the large q limit. In the next subsection we will derive a differential equation for $g(\mu,\tau)$ and subsequently solve it.

Let us now see what becomes of the Schwinger Dyson equations in the presence of the chemical potential and a q point random all to all interaction. We have,

$$G(\mu,\omega) = \frac{1}{-i\omega + \mu - \Sigma(\mu,\omega)} . \tag{1.1.33}$$

$$\Sigma(\mu,\tau) = J^2 \left(G(\mu,\tau)\right)^{q/2} \left(G(\mu,-\tau)\right)^{q/2-1} . \tag{1.1.34}$$

When $\mu = 0$ and we go to the IR limit we see that the above two equations can be solved self consistently by using a reparametrization ansatz,

$$G_c(\tau) = b\frac{\text{sgn}(\tau)}{|\tau|^{\frac{2}{q}}} . \tag{1.1.35}$$

Notice that if we have $J^2 >> \mu$ then also this solution holds. But let us now rewrite this expression as an expansion in $1/q$,

$$G_c(\tau) = b\text{sgn}(\tau)\left(1 - \frac{2\log|\tau|}{q} + ..\right) . \tag{1.1.36}$$

This is fairly easy to see and gives us the idea that in the large q the two point function can indeed be expanded in such a series (1.1.29) where the function appearing as a coefficient of the $1/q$ term (i.e. $g(\mu,\tau)$) approaches $-2\log|\tau|$ in the IR and at zero temperature.

1.1.4 Differential equation for $g(\mu,\tau)$

To derive the desired differential equation, we follow a simple generalisation of the method discussed in [21]. First, note that, in the large N limit, all melonic Feynman diagram can be summed up to obtain the following Schwinger-Dyson equation:

$$\frac{1}{G(\mu,\omega)} = i\omega + \mu - \Sigma(\omega,\mu) , \tag{1.1.37}$$

$$\Sigma(\mu,\tau) = J^2(-1)^{q/2}(G(\mu,\tau))^{q/2}(G(\mu,-\tau))^{q/2-1} . \tag{1.1.38}$$

It is straightforward to derive the first Schwinger-Dyson equation by summing up the one particle irreducible diagrams. Also it is straightforward to verify the second equation above by looking at the melonic diagrams. Each propagator in this diagram is the two point function of the full interacting theory i.e. each propagator themselves contain such melonic contributions, see figure 1.2.

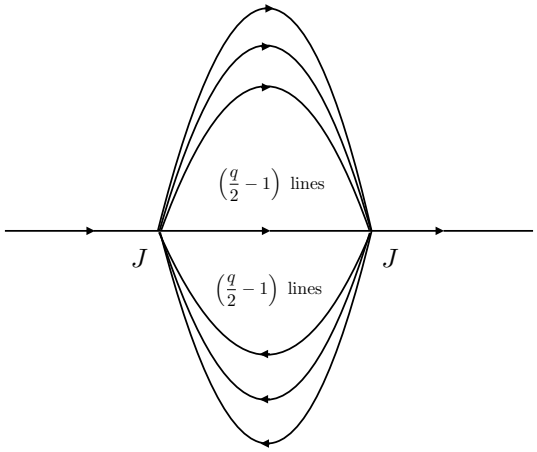

$$\Sigma \sim J^2 G\left(\mu,\tau\right)^{\frac{q}{2}} G\left(\mu,-\tau\right)^{\frac{q}{2}-1}$$

Figure 1.2: A diagrammatic representation of Σ. Each vertex is worth of strength J, and $\left(\frac{q}{2}-1\right)$ propagators run inside the loop in each direction. The direction of the arrows correlate with the sign of τ in the argument of the propagators. The overall direction of the diagram, from left to right, selects out two additional propagators running in this direction and hence the corresponding powers of G.

These Schwinger-Dyson equations take especially simple form in the $q \to \infty$ limit. In particular, the function $g(\mu,\tau)$ in this limit appears in the exponential:

$$\frac{1}{G(\mu,\omega)} = i\omega + \mu - (i\omega+\mu)^2 \frac{f * g(\mu,\omega)}{2q} \,. \tag{1.1.39}$$

$$\Sigma(\mu,\tau) = \frac{J^2 G_0(\mu,\tau)}{(2+2\cosh(\mu\beta))^{q/2-1}} e^{\frac{1}{2}(g(\mu,\tau)+g(\mu,-\tau))} \,. \tag{1.1.40}$$

We can now identify the self energy contribution to the inverse propagator as the Fourier transform of $\Sigma(\mu,\tau)$ appearing in (1.1.37). Taking the inverse Fourier transform of the self energy contribution in (1.1.39) we get the differential equation:

$$(\partial_t - \mu)^2 \left[G_0(\mu,\tau) g(\mu,\tau)\right] = 2\frac{q J^2 G_0(\mu,\tau)}{2(2+2\cosh(\mu\beta))^{q/2-1}} e^{\frac{1}{2}(g(\mu,\tau)+g(\mu,-\tau))} \,. \tag{1.1.41}$$

For $\tau > 0$ this equation reduces to:

$$\partial_\tau^2 g(\mu,\tau) = 2\tilde{J}^2 e^{\frac{1}{2}(g(\mu,\tau)+g(\mu,-\tau))} \,, \tag{1.1.42}$$

where,

$$\tilde{J}^2 = \frac{qJ^2}{2(2+2\cosh(\mu\beta))^{\frac{q}{2}-1}} \,. \tag{1.1.43}$$

It is worth pointing out at this point that this differential equation is quite similar to that appearing in [21]. We will solve this equation analytically in the next section.

Before moving further, a few comments regarding the large q result are in order. It is straightforward to check that, if one goes beyond the leading order in $(1/q)$-expansion, the Schwinger-Dyson equation again rearranges itself to the differential equation of the type discussed above, with the same effective coupling $\tilde{J}$.

To see this explicitly let us first notice that the μ dependence of $\tilde{J}$ comes only from the free part. If we look at the behavior of the self-energy contribution at $O(\frac{1}{q^2})$ we find for $\mu = 0$ case, the terms take the form

$$J^2\left(1+\frac{g(\tau)}{q}+\frac{g'(\tau)}{q^2}+...\right)^{q-1} \,. \tag{1.1.44}$$

The equation for function g' cannot be obtained by simply exponentiating it, as was done for the leading correction, namely $g(\tau)$. We instead have an asymptotic series expansion in $\frac{1}{q}$. Now if we turn on finite μ then from the self-energy expression we get,

$$\frac{J^2}{2(2+2\cosh(\mu\beta))^{q/2-1}}\left(1+\frac{g(\mu,\tau)}{q}+\frac{g'(\mu,\tau)}{q^2}+..\right)^{\frac{q}{2}}\left(1+\frac{g(\mu,-\tau)}{q}+\frac{g'(\mu,-\tau)}{q^2}+..\right)^{\frac{q}{2}-1} \,. \tag{1.1.45}$$

The form is exactly like in the SYK model. As a result the equation that we would obtain in this case will be identical to that for g' in the SYK model. In other words even for finite μ, the effective coupling constant $\tilde{J}$ remains unaltered even at higher order in $1/q$. The emergence of one effective coupling is an inherent feature of this asymptotic expansion in $(1/q)$.

1.2 The six point function preliminaries

In this section we look at some preliminary facts on the six point function which we will elaborate on later in chapter 3. If we do a large N analysis then from the $1/N$ expansion of the six point function is given by,

$$\frac{1}{N^3}\sum_{i,j,k=1}^{N}\left\langle\psi_i^\dagger(\tau_1)\psi_i(\tau_2)\psi_j^\dagger(\tau_3)\psi_j(\tau_4)\psi_k^\dagger(\tau_5)\psi_k(\tau_6)\right\rangle = G(\tau_{12})G(\tau_{34})G(\tau_{56})$$
$$+\frac{1}{N}\left(G(\tau_{12})\mathcal{F}(\tau_3,\tau_4,\tau_5,\tau_6)+G(\tau_{34})\mathcal{F}(\tau_1,\tau_2,\tau_5,\tau_6)+G(\tau_{56})\mathcal{F}(\tau_1,\tau_2,\tau_3,\tau_4)\right)+\frac{1}{N^2}\mathcal{S}(\tau_1,...,\tau_6) \,. \tag{1.2.1}$$

Here $\mathcal{S}$ denotes the fully connected component of the six point function. Since we are working in the large N limit the only contributions to the fully connected piece comes from what are known as the “Contact" and the “Planar" diagrams.

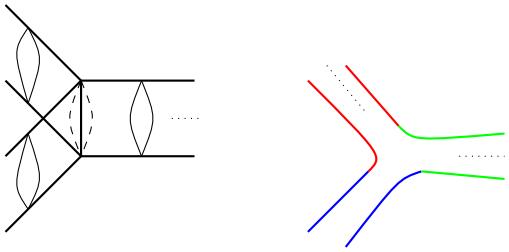

Figure 1.3: The “Contact" and “Planar" diagrams respectively. The dots denote that there are rungs connecting the legs of the same colour in the “Planar" diagram. (Adapted from [18, 48], drawn using package tikz.)

We thus have for the “Contact" diagrams,

$$S_c = (q-1)(q-2)J^2 \int d\tau_a d\tau_b G(\tau_{ab})^{\frac{q}{2}-3} G(-\tau_{ab})^{\frac{q}{2}} \mathcal{F}(\tau_1,\tau_2,\tau_a,\tau_b)\mathcal{F}(\tau_3,\tau_4,\tau_a,\tau_b)\mathcal{F}(\tau_5,\tau_6,\tau_a,\tau_b)\,. \tag{1.2.2}$$

While the “Planar" contribution goes as,

$$\mathcal{S}_p = \int_{-\infty}^{\infty} d\tau_a d\tau_b d\tau_c \mathcal{F}_{\text{amp}}(\tau_1,\tau_2,\tau_a,\tau_b)\mathcal{F}_{\text{amp}}(\tau_4,\tau_3,\tau_c,\tau_a)\mathcal{F}_{\text{amp}}(\tau_5,\tau_6,\tau_b,\tau_c)\,, \tag{1.2.3}$$

where,

$$\mathcal{F}_{\text{amp}}(\tau_1,\tau_2,\tau_3,\tau_4) = -\int_0^\beta d\tau_0 \mathcal{F}(\tau_1,\tau_2,\tau_3,\tau_0) \int \frac{d\omega_4}{2\pi} e^{-i\omega_4\tau_{40}} \frac{1}{G(\mu,\omega_4)}\,.$$

And $\mathcal{S} = \mathcal{S}_c + \mathcal{S}_p$, is the full contribution to the fully connected piece of the six point function.

2 Tuning of Chaos Behavior

In this chapter we study the SYK model with complex fermions, in the presence of an all-to-all q-body interaction, with a non-vanishing chemical potential. We find that, in the large q limit, this model can be solved exactly and the corresponding Lyapunov exponent can be obtained semi-analytically. The resulting Lyapunov exponent is a sensitive function of the chemical potential μ. Even when the coupling J, which corresponds to the disorder averaged values of the all to all fermion interaction, is large, values of μ which are exponentially small compared to J lead to suppression of the Lyapunov exponent.

This chapter is divided in the following sections: In section 2.1, we discuss the calculation of the retarded kernel. We will first have to compute the retarded Green's function. Section 2.2 is devoted to studying the dependence of the Lyapunov exponent on μ, in details. We comment briefly on flavoured complex fermion model in section 2.3.

2.1 Calculating the retarded kernel

Let us begin by computing the retarded kernel. We are going to find the expression of the kernel with all its components analytically continued to real time. Our goal is to find the eigen-function of this retarded kernel with eigenvalue 1. But for this purpose we need to figure out what will be the retarded two point function and the Wightman correlator.

Notice that the right hand side of the differential equation (1.1.42) is symmetric under $\tau \to -\tau$, whereas on the left hand side we switch from $g(\mu,\tau) \to g(\mu,-\tau)$. We can therefore send $\tau \to -\tau$, and subsequently obtain the resulting equation for $g(\mu,-\tau)$. The solutions to the differential equations are exactly of the Maldacena-Stanford form [21], and are given by

$$e^{g(\mu,\tau)} = \frac{\cos^2\left(\frac{\pi\nu}{2}\right)}{\cos^2\left(\pi\nu\left(\frac{|\tau|}{\beta}-\frac{1}{2}\right)\right)}\,, \quad \text{with} \quad \beta\tilde{J} = \frac{\pi\nu}{\cos\left(\frac{\pi\nu}{2}\right)}\,. \tag{2.1.1}$$

Note that, the parameter ν that naturally emerges here contains information about the two independent UV-couplings: βJ and $\beta\mu$.

2.1.1 The retarded Green's function

We begin by defining the retarded Green's function

$$G_{\mathrm{R}}(\mu,t)=\lim_{\epsilon\to 0+}\left[G_{>}(\mu,it+\epsilon)-G_{<}(\mu,it-\epsilon)\right]\Theta(t)\,. \tag{2.1.2}$$

In the $q\to\infty$ limit, we obtain:

$$G_{\mathrm{R}}(\mu,t)=-e^{i\mu t}\Theta(t)\,. \tag{2.1.3}$$

The above result, in the limit $\mu\to 0$, yields: $G_{\mathrm{R}}(t)=\Theta(t)$ which is the expected answer. We can also define:

$$G_{\mathrm{R}}(\mu,-t)=\lim_{\epsilon\to 0+}\left[G_{>}(\mu,-(it+\epsilon))-G_{<}(\mu,-(it-\epsilon))\right]\Theta(t)\,, \tag{2.1.4}$$

which implies $G_{\mathrm{R}}(\mu,-t)=e^{-i\mu t}\Theta(t)$.

2.1.2 The retarded kernel

Now we analyze the four-point function. In the large N limit, the four-point function can be expanded in a series of $(1/N)$ and, here, we will only compute the the leading $(1/N)$-contribution, in which only the ladder diagrams contribute. Since we are working with complex fermions, the only non-trivial four-point function is given by

$$\frac{1}{N^2}\sum_{i,j=1}^{N}\left\langle T\left(\psi_i(t_1)\psi_i^{\dagger}(t_2)\psi_j^{\dagger}(t_3)\psi_j(t_4)\right)\right\rangle=G(t_{12})\,G(t_{34})+\frac{1}{N}\mathcal{F}(t_1,t_2,t_3,t_4)+\ldots \tag{2.1.5}$$

The contribution at order $(1/N)$ is collectively denoted by $\mathcal{F}=\sum_n\mathcal{F}_n$, where n is the number of rungs in the corresponding ladder diagram. We refer to [21] for more details. The composition rule is pictorially represented in figure 2.1.

At large N, the summation over the ladder diagrams can be performed by expressing $\mathcal{F}_{n+1}$ in terms of $\mathcal{F}_n$ integrated, weighted with a kernel, as also pictorially shown in figure 2.1:

$$\mathcal{F}_{n+1}(t_1,t_2,t_3,t_4)=\int dtdt'\,K_{\mathrm{R}}(t_1,t_2;t,t')\,\mathcal{F}_n(t,t',t_3,t_4)\,, \tag{2.1.6}$$

where the kernel, denoted above by K_{R}, is given by

$$K_{\mathrm{R}}(t_1,t_2,t_3,t_4)=(-1)^{q/2}J^2(q-1)\qquad \begin{aligned}&G_{\mathrm{R}}(\mu,t_{13})\,G_{\mathrm{R}}(\mu,-t_{24})\\ &\left[G_{\mathrm{lr}}(\mu,t_{34})\right]^{q/2-1}\left[G_{\mathrm{lr}}(\mu,-t_{34})\right]^{q/2-1}\end{aligned}\,. \tag{2.1.7}$$

Here $G_{\mathrm{lr}}(\mu,t)$ is the Wightman function, which is essentially given by the propagator evaluated at complex time, and in the large q limit we get:

$$\left[G_{\mathrm{lr}}(t)\right]^{q/2-1}\left[G_{\mathrm{lr}}(-t)\right]^{q/2-1}=\left[G(it+\beta/2)\right]^{q/2-1}\left[G(-it-\beta/2)\right]^{q/2-1}\,. \tag{2.1.8}$$

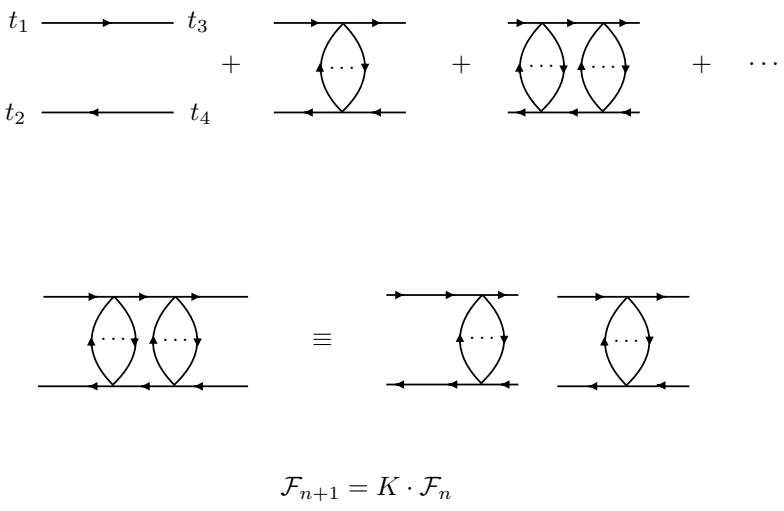

Figure 2.1: A diagrammatic representation of the four point function calculation, in the large N limit. First, only the ladder diagrams contribute, as shown in the first row here. Second, from the structure of the diagrams, one obtains an iterative process to generate $\mathcal{F}_{n+1}$ from $\mathcal{F}_n$, composing with a kernel.

The above is consistent with interpreting the propagator $G(\mu, -t)$ as the fermion moving backward in time, or the anti-fermion moving forward in time. This is why a separation along the thermal circle picks up a relative sign.

Finally, we obtain:

$$(-1)^{q/2} J^2 (q-1) \left[G_{\rm lr}(t)\right]^{q/2-1} \left[G_{\rm lr}(-t)\right]^{q/2-1} = (-1)^{q-1} \frac{2\pi^2 \nu^2}{\beta^2 \cosh^2\left(\frac{\pi \nu t}{\beta}\right)} \,. \tag{2.1.9}$$

Using this, the complete retarded kernel is given by

$$K_{\rm R}(t_1, t_2, t_3, t_4) = -(-1)^{q-1} e^{i\mu(t_{13}-t_{24})} \frac{2\pi^2 \nu^2 \Theta(t_{13}) \Theta(t_{24})}{\beta^2 \cosh^2\left(\frac{\pi \nu t_{34}}{\beta}\right)} \tag{2.1.10}$$

$$= e^{i\mu(t_{12}-t_{34})} \frac{2\pi^2 \nu^2 \Theta(t_{13}) \Theta(t_{24})}{\beta^2 \cosh^2\left(\frac{\pi \nu t_{34}}{\beta}\right)} \,. \tag{2.1.11}$$

The last equality follows from the fact that q is even.

2.2 Exploring the chaos regime

So far, we have obtained the retarded kernel for four fermion fields placed at four arbitrary points on the thermal circle, denoted respectively by $t_1, \ldots, t_4$. To extract the chaos be-

haviour, one needs to calculate the OTO correlation in real time, separating the fermions by a quarter of the thermal circle [50]. We want to compute the following OTO correlation:

$$\mathcal{F}(t_1,t_2) = \mathrm{Tr}\left[y\psi_i(t_1)y\psi_i^\dagger(0)y\psi_j^\dagger(t_2)y\psi_j(0)\right] , \quad y=\rho(\beta)^{1/4} . \tag{2.2.1}$$

In the limit $t_1, t_2 \to \infty$, the diagram with zero rung is suppressed and thus $\mathcal{F}(t_1,t_2)$ is an eigenfunction of the retarded kernel K_{R}, with an eigenvalue one. This statement translates into an integral equation of the following form:

$$\begin{aligned}\mathcal{F}(t_1,t_2) &= \int_{-\infty}^{\infty}\int_{-\infty}^{\infty} dt_3 dt_4 K_{\mathrm{R}}(t_1,t_2,t_3,t_4)\mathcal{F}(t_3,t_4) &(2.2.2)\\ &= \int_{-\infty}^{\infty}\int_{-\infty}^{\infty} dt_3 dt_4 e^{i\mu(t_{12}-t_{34})}\frac{2\pi^2\nu^2\Theta(t_{13})\Theta(t_{24})}{\beta^2\cosh^2\left(\frac{\pi\nu t_{34}}{\beta}\right)}\mathcal{F}(t_3,t_4) . &(2.2.3)\end{aligned}$$

Choosing an exponential-ansatz for $\mathcal{F}(t_3,t_4)$ of the form

$$\mathcal{F}(t_3,t_4) = e^{\frac{\pi\nu}{\beta}(t_3+t_4)}\frac{e^{i\mu t_{34}}}{\cosh\left(\frac{\pi\nu t_{34}}{\beta}\right)} , \tag{2.2.4}$$

yields:

$$\begin{aligned}\mathcal{F}(t_1,t_2) &= e^{i\mu t_{12}}\int_{-\infty}^{t_1}\int_{-\infty}^{t_2} dt_3 dt_4 \frac{2\pi^2\nu^2 e^{\frac{\pi\nu}{\beta}(t_3+t_4)}}{\beta^2\cosh^3\left(\frac{\pi\nu t_{34}}{\beta}\right)} &(2.2.5)\\ &= e^{\frac{\pi\nu}{\beta}(t_1+t_2)}\frac{e^{i\mu(t_{12})}}{\cosh\left(\frac{\pi\nu t_{12}}{\beta}\right)} . &(2.2.6)\end{aligned}$$

This implies, following the subsequent steps outlined in [21], that the Lyapunov exponent is given by

$$\lambda_{\mathrm{L}} = \frac{2\pi}{\beta}\nu , \tag{2.2.7}$$

where ν is given in equation (2.1.1). In the two extreme limits, we easily get:

$$\begin{aligned}\lambda_{\mathrm{L}} &= \left(2\tilde{J}\right) + \ldots , \quad \text{as} \quad \nu \to 0 \quad \Longleftrightarrow \quad \beta\tilde{J} \to 0 , &(2.2.8)\\ &= \frac{2\pi}{\beta}\left(1-\frac{2}{\beta\tilde{J}}\right) , \quad \text{as} \quad \nu \to 1 \quad \Longleftrightarrow \quad \beta\tilde{J} \to \infty . &(2.2.9)\end{aligned}$$

In terms of the IR emergent coupling $\beta\tilde{J}$, the dependence is identical to the one observed in [21], however, in terms of the original parameters $\{\beta J, \beta\mu\}$ defining the system, there is a non-trivial dependence of the Lyapunov exponent. The figure 2.2, shows behaviour of $\lambda = \beta\lambda_L/2\pi$, which is the normalised Lyapunov exponent, as a function of the coupling βJ for various values of $\beta\mu$. Similarly the figure 2.3 shows variation of λ as a function of $\beta\mu$ for different values of βJ.

To compare with the results obtained in [22] we can also plot the Figure 2.4 using our formula.

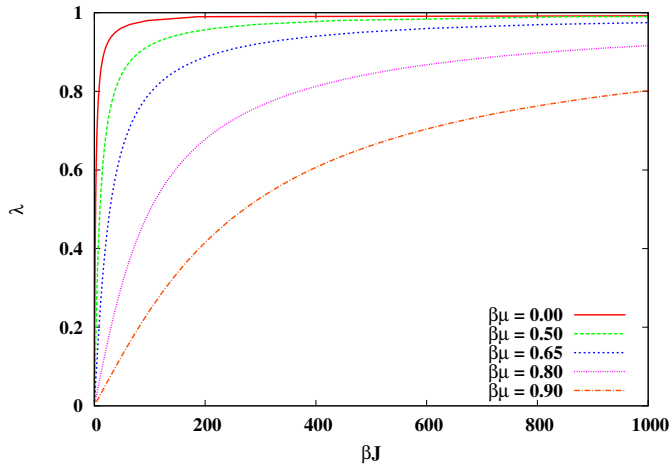

Figure 2.2: The Lyapunov exponent λ is normalised and takes values between 0 and 1. This figure shows dependence of λ on βJ for different values of $\beta\mu$.

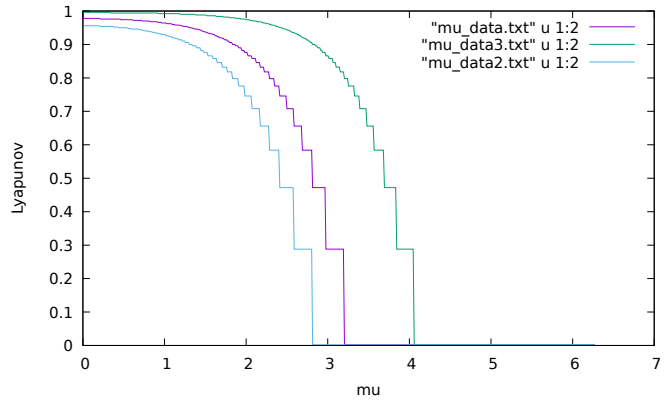

Figure 2.3: The Lyapunov exponent λ is again normalised and takes values between 0 and 1. This figure shows dependence of λ on $\beta\mu$ for different values of βJ.

Before concluding this section, let us make some comments regarding tuning the chaotic properties of SYK-type models. In [22], a two-body infinite-range random interaction between Majorana fermions was introduced, in addition to the four-fermi interaction in the SYK model. It was found that this interaction can tune the Lyapunov exponent down, and in fact, push it all the way to zero, similar to what we have observed above. However, the precise dependence of the Lyapunov exponent with the one-body interaction strength is different compared to our results.

The Hamiltonian considered in [22] is of the following form:

$$H = \sum_{1\le i_1\le i_2\le i_3\le i_4\le N} J_{i_1 i_2 i_3 i_4}\ \psi_{i_1}\psi_{i_2}\psi_{i_3}\psi_{i_4} + i \sum_{1\le i_1\le i_2\le N} k_{i_1 i_2}\ \psi_{i_1}\psi_{i_2}\ , \tag{2.2.10}$$

where $J_{i_1 i_2 i_3 i_4}$ are chosen from a familiar Gaussian ensemble, and the couplings $k_{i_1 i_2}$ denote the infinite-range interaction and ψ_i's are Majorana fermions. Assuming N is even, we can consider a particularly special case, in which $k_{i_1 i_2}$ are non-random, and are characterized

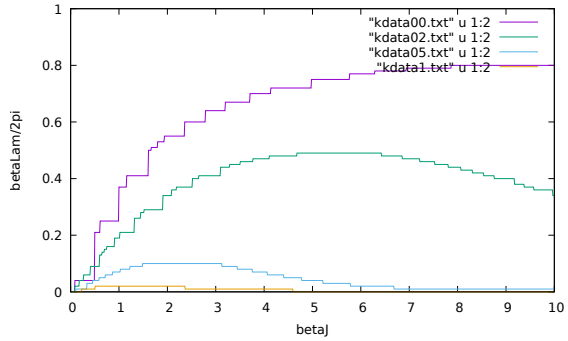

Figure 2.4: Plot of $\frac{\lambda_L \beta}{2\pi}$ against βJ with $q = 10$. The plots are with respect to $\kappa = 0.1, 0.2, 0.5, 1$, where $J \to \frac{J}{\kappa}$ and $\mu \to \mu\kappa$

by a particularly nearest neighbour interaction:

$$\begin{aligned} k_{i_1 i_2} &= k\delta_{i_1+1,i_2} \quad \text{if} \quad i_1 = \text{odd}\,, \\ &= 0 \quad \text{otherwise}\,. \end{aligned} \tag{2.2.11}$$

The interaction term is now particularly simple:

$$H_{\text{int}} = i \sum_{i=\text{odd}}^{N} k_{i,i+1}\, \psi_i \psi_{i+1} \equiv \Psi^\dagger \mathcal{K} \Psi\,, \tag{2.2.12}$$

$$\text{where} \quad \Psi^\dagger = (\psi_1, \psi_2, \ldots \psi_N)\,. \tag{2.2.13}$$

Evidently, the † operation is equivalent to the transpose operation since we are dealing with Majorana fermions. The matrix $\mathcal{K}$ contains the information about the nearest-neighbour interaction of (2.2.11). It is easy to diagonalize the coupling matrix $\mathcal{K}$, and the resulting eigenvalues are: $\left(\frac{N}{2}\right)$ copies of $\left(+\frac{k}{2}\right)$ and $\left(\frac{N}{2}\right)$ copies of $-\left(\frac{k}{2}\right)$. Suppose that χ^+_a, with $a = 1, \ldots, N/2$, eigenvectors have positive eigenvalues and χ^-_a, with $a = 1, \ldots, N/2$, eigenvectors have negative eigenvalues. It is also straightforward to check that: $(\chi^+)^\dagger = \chi^-$, thus we can drop the superscript, and subsequently the interaction term can be written as:

$$H_{\text{int}} = k \sum_{a}^{N/2} \chi^\dagger_a \chi_a\,, \quad \text{where} \quad \left\{\chi^\dagger_a, \chi_b\right\} = 2\delta_{ab}\,. \tag{2.2.14}$$

We can now rewrite the four-body interaction in the complex χ-basis. Since our starting point did not preserve the U(1)-symmetry of the complex fermion model in (1.1.10), the full resulting Hamiltonian does not match with the complex fermion model with $q = 4$. However, in the UV, with $(J/k) \to 0$, the four-point interaction is negligible and the two systems are physically equivalent. In the IR, the two systems are completely distinct.

2.3 Flavoured Complex fermions with a chemical potential

Let us now generalise this set up, where instead of a U(1) symmetry we have N_f number of flavoured fermions with a global SU(N_f) flavour symmetry, similar to the model considered in [25]. The fermions now carry two indices, Ψ_i^α. Here the α is the flavour index where as i is the site index. One has the following operator algebra:

$$\{\Psi_i^\alpha, \Psi_j^\beta\} = \{\Psi_i^{\alpha\dagger}, \Psi_j^{\beta\dagger}\} = 0\,, \quad \{\Psi_i^\alpha, \Psi_j^{\beta\dagger}\} = \delta_{ij}\delta^{\alpha\beta}\,. \tag{2.3.1}$$

It is a trivial matter to find first the kinetic term without introducing the chemical potential μ it given by

$$-\int d\tau \Psi_i^{\alpha\dagger}\partial_\tau \Psi_i^\alpha\,. \tag{2.3.2}$$

Here repeated indices are summed over unless stated otherwise.

The SU(N_f) invariant two point function in this case will be given by

$$G(\tau) = \langle \Psi_i^\alpha(\tau)\Psi_j^{\alpha\dagger}(0)\rangle \equiv \frac{N_f \mathrm{sgn}(\tau)}{2}\delta_{ij}\,. \tag{2.3.3}$$

If we absorb this factor of N_f into the overall normalization of the kinetic piece then we observe that now if one introduces a conserved charge μ then the relevant operator is:

$$\frac{\mu}{N_f}\Psi_i^\alpha \Psi_i^{\alpha\dagger}.$$

We know that the interaction term should be a gauge singlet. We also require that, upon imposing reality condition on the fermions, this interaction should reduce to the corresponding interaction term in the Gross-Rosenhaus model. Under this, we intuitively write down the interaction term as:

$$\frac{1}{N_f^{q/2}} J_{i_1\ldots i_q}\Psi_{i_1}^{\alpha_1\dagger}\ldots\Psi_{i_{q/2}}^{\alpha_{q/2}\dagger}\Psi_{i_{q/2+1}}^{\alpha_{q/2}}\ldots\Psi_{i_q}^{\alpha_1}\,. \tag{2.3.4}$$

Now we just use the melon diagrams to figure out the 1PI effective self energy contribution. Essentially, as before, we observe that from the diagramatics one obtains:

$$\Sigma(\tau) = \frac{C_{\frac{q}{2}}^{N_f}}{N_f^q} J^2\,[G(\tau)]^{q/2}\,[G(-\tau)]^{q/2-1}\,.$$

So, one can redefine the coupling strength as: $J_{\text{eff}}^2 = \frac{C_{\frac{q}{2}}^{N_f}}{N_f^q} J^2$. This means that, if we have multiple groups of flavours, then the relative strength of the effective couplings scale according to the above relation. Hence, again we get back the same set of Schwinger-Dyson equations which we have already solved.

We already see the emergence of an effective coupling:

$$J_{\text{eff}}^2 = \frac{1}{N_f^q} \frac{N_f!}{\left(\frac{q}{2}\right)! \left(N_f - \frac{q}{2}\right)!} J^2 \,, \tag{2.3.5}$$

which, in the limit $q \gg 1$, $N_f \gg 1$ such that $N_f \gg q$, naively, yields:

$$J_{\text{eff}}^2 = \frac{1}{N_f^q} \frac{1}{\left(\frac{q}{2}\right)!} J^2 \to 0 \,. \tag{2.3.6}$$

Thus, with a very large global symmetry, the emergent coupling is very weak. This implies that the resulting chaotic behaviour will be accompanied with a vanishingly small value of the Lyapunov exponent. Thus, we can tune the chaotic behaviour with a global flavour symmetry, as well.

3 Chaotic Correlation Function

In the standard SYK model, in the large q limit, the relevant scale in the system is provided by an effective coupling:

$$\mathcal{J} = \frac{qJ^2}{2^{q-1}} ,$$

which has mass dimension one. The IR CFT resides in the $\mathcal{J} \to \infty$ limit, but the exponential growth of OTOC and subsequently the Lyapunov exponent can be obtained as a perturbation series in $1/\mathcal{J}$. This naturally gives an RG-flow of the Lyapunov exponent [21]. In the previous chapter we saw how the maximally chaotic mode of the SYK model with complex fermions in the large q limit behave in the presence of a chemical potential μ. Here, in the UV Hamiltonian, we have two natural parameters: $\beta\mu$ and $\beta\mathcal{J}$ and the effective coupling in the IR is given by (This is the same as in (1.1.43) with $\tilde{J}$ from here on denoted as)

$$\mathcal{J}_{\text{eff}}^2 = \frac{q}{2} \frac{J^2}{(2 + 2\cosh(\mu\beta))^{\frac{q}{2}-1}} . \tag{3.0.1}$$

The strict IR is located at $\mathcal{J}_{\text{eff}} \to \infty$ limit, and one can calculate systematically the RG-flow of the Lyapunov exponent in a perturbation series in $1/\mathcal{J}_{\text{eff}}$. This RG-flow shows sensitive behaviour for the Lyapunov exponent as the UV parameter $\beta\mu$ is dialled up as we saw in 2.2.

In keeping with the theme, in this article, we further compute higher point OTOC for complex fermion SYK-model, with a non-vanishing chemical potential. Our analyses follow closely the analyses in [48], in the large q limit. However, our analyses are performed in the complementary regime in that we completely focus on the operators that display chaotic nature and away from the conformal limit. In spirit of the NAdS/NCFT picture, this is rather natural regime to consider; in the context of chaotic properties of many body systems, this is an example of a tractable and explicit higher point OTOC which displays the expected exponential growth.

In this paper, after computing the fermion six point function with a non-vanishing chemical potential, we take the triple short time limit to estimate the the bulk three point correlator, away from the conformal limit. In this regard, we compute bulk three point function(triple short time limit of the fermion six point correlators, neglecting the Schwarzian

mode) of the modes satisfying conformal invariance as well as the Schwarzian mode, using the techniques employed by Gross and Rosenhaus [48].

This chapter is organized as follows. In section 3.1, we compute the six point fermion correlator in the triple short time limit for the conformal modes in the IR limit i.e. μ turned off. We then interpret it in terms of the bulk three point correlator [48, 49] in the IR limit of the conformal modes and check that we do indeed find them to be of the form of conformal three-point function, in the triple short time limit. We apply this technique in Section 3.2 to compute the six point function and take the triple short time limit to determine the three point correlation function of fermion bilinears away from the conformal limit. These computations in the presence of a chemical potential μ which only affects the correlation functions through the effective coupling. We also numerically plot the OTO configuration with changing time and attempt to extract the chaos exponent.

3.1 Correlation Functions

Let us begin with the short time *i.e.*, $\tau_1 - \tau_2 = \tau_{12} \to 0$ limit of the four point function both for the symmetric and anti-symmetric case,

$$\begin{aligned} F^A(\tau_1,\tau_2,\tau_3,\tau_4) =& G(\tau_{12})G(\tau_{34})\sum_{n=1}^{\infty} c_n^2\left(\frac{|\tau_{12}\tau_{34}|}{|\tau_{13}\tau_{14}|}\right)^{h_n}, \\ F^S(\tau_1,\tau_2,\tau_3,\tau_4) =& G(\tau_{12})G(\tau_{34})\sum_{n=1}^{\infty} \tilde{c}_n^2\left(\frac{|\tau_{12}\tau_{34}|}{|\tau_{13}\tau_{14}|}\right)^{h_n}, \end{aligned} \tag{3.1.1}$$

When we calculate the the six point function of the complex fermions we go to different short time limits, where the correlation function take some effective form. In the triple short time limit we calculate it as an effective three point function of the fermion bi-linear operators. This way one can compute the correlation function near points where different arguments approach each other yielding poles and by the property of being analytic everywhere else we get the full contribution.

In the remaining part of this article we calculate the $O(1/N^2)$ coefficient of the six point function with respect to the $1/N$ expansion. To this order there are contributions from the contact diagrams as well planar diagrams. We will now write down the corresponding expressions:

$$\mathcal{S} = \mathcal{S}_1 + \mathcal{S}_2 + \tilde{\mathcal{S}}_1 + \tilde{\mathcal{S}}_2. \tag{3.1.2}$$

Here the contributions of $\mathcal{S}_1$ (contact) and $\mathcal{S}_2$ (planar) are exactly same as in [48], namely the result for the Majorana fermions. In case of the SYK model with complex fermions, if we demand time reversal invariance, (since the Hamiltonian is itself time reversal invariant) we have only two other contributions. Now,

$$\frac{\tilde{\mathcal{S}}_1}{90} = (q-1)(q-2)J^2 \iint_{-\infty}^{\infty} d\tau_a d\tau_b G(\tau_{ab})^{q-3} F^S(\tau_1,\tau_2,\tau_a,\tau_b)F^A(\tau_3,\tau_4,\tau_a,\tau_b)F^S(\tau_5,\tau_6,\tau_a,\tau_b), \tag{3.1.3}$$

is the contact diagram contribution. Here, we have written only one particular assignment of the arguments; there are other possible assignments whose contributions account for the factor of $1/90$ on the left hand side. There are total 90 possible independent configurations. We will use same symbol h to denote the conformal weight of the bilinear operators both for F^A and F^S, although the values are different for the two: for $F^A \Rightarrow h_n = 2n + 1 + 2\Delta + O\left(\frac{1}{k}\right)$, and for $F^S \Rightarrow h_n = 2n + 2\Delta + O\left(\frac{1}{k}\right)$. Also we have,

$$\frac{\tilde{S}_2}{90} = \int_{-\infty}^{\infty} d\tau_a d\tau_b d\tau_c \mathcal{F}^S_{amp}(\tau_1, \tau_2, \tau_a, \tau_b)\mathcal{F}^A_{amp}(\tau_3, \tau_4, \tau_b, \tau_c)\mathcal{F}^S_{amp}(\tau_5, \tau_6, \tau_c, \tau_a) \,, \tag{3.1.4}$$

where,

$$\mathcal{F}^S_{amp}(\tau_1, \tau_2, \tau_3, \tau_4) = J^2 \int d\tau_0 F^S(\tau_1, \tau_2, \tau_3, \tau_0) G(\tau_{40})^{q-1} \,. \tag{3.1.5}$$

Using the Selberg integrals in its special and general forms, one obtains:

$$\mathcal{F}^S_{amp}(\tau_1, \tau_2, \tau_3, \tau_4) = G(\tau_{12}) \sum_n \tilde{c}_n^2 \tilde{\xi}_n sgn(\tau_{12}) sgn(\tau_{43}) \frac{|\tau_{12}|^{h_n} |\tau_{34}|^{h_n - 1}}{|\tau_{24}|^{h_n + 1 - 2\Delta} |\tau_{23}|^{h_n - 1 + 2\Delta}} \,. \tag{3.1.6}$$

Using the short time expansion of four point amplitudes, we get:

$$\begin{aligned}
\frac{\tilde{S}_1}{90} =& b^q (q-1)(q-2) J^2 \sum_{n,m,k} \tilde{c}_n c_m \tilde{c}_k |\tau_{12}|^{h_n} |\tau_{34}|^{h_m} |\tau_{56}|^{h_k} G(\tau_{12}) G(\tau_{34}) G(\tau_{56}) I^{(1)}_{nmk} \,, \\
\frac{\tilde{S}_2}{90} =& b^q (q-1)(q-2) J^2 \sum_{n,m,k} \tilde{c}_n c_m \tilde{c}_k \tilde{\xi}_n \xi_m \tilde{\xi}_k |\tau_{12}|^{h_n} |\tau_{34}|^{h_m} |\tau_{56}|^{h_k} \\
& \times G(\tau_{12}) G(\tau_{34}) G(\tau_{56}) I^{(2)}_{nmk} \,,
\end{aligned} \tag{3.1.7}$$

where explicit expressions of the constants c, ξ, $\tilde{c}$, $\tilde{\xi}$ are given in appendix 3.4. The integrals $I^{(1)}$ and $I^{(2)}$ are given by

$$I^{(1)}_{nmk}(\tau_1, \tau_3, \tau_5) = \text{sgn}(\tau_{12})\text{sgn}(\tau_{56}) \int_{-\infty}^{\infty} d\tau_a \, d\tau_b \frac{\text{sgn}(\tau_{1a}\tau_{1b}\tau_{5a}\tau_{5b}) |\tau_{ab}|^{h_n + h_m + h_k - 2}}{|\tau_{1a}|^{h_n} |\tau_{1b}|^{h_n} |\tau_{3a}|^{h_m} |\tau_{3b}|^{h_m} |\tau_{5a}|^{h_k} |\tau_{5b}|^{h_k}} \,, \tag{3.1.8}$$

$$\begin{aligned}
I^{(2)}_{nmk}(\tau_1, \tau_3, \tau_5) = -\text{sgn}(\tau_{12})\text{sgn}(\tau_{56}) \int_{-\infty}^{\infty} d\tau_a \, d\tau_b \, d\tau_c \Bigg[& \frac{\text{sgn}(\tau_{3b})\text{sgn}(\tau_{3c})}{|\tau_{3c}|^{h_m - 1 + 2\Delta} |\tau_{3a}|^{h_m + 1 - 2\Delta}} \\
& \times \frac{\text{sgn}(\tau_{ab})\text{sgn}(\tau_{bc}) |\tau_{ab}|^{h_n - 1} |\tau_{ca}|^{h_m - 1} |\tau_{bc}|^{h_k - 1}}{|\tau_{1a}|^{h_n - 1 + 2\Delta} |\tau_{1b}|^{h_n + 1 - 2\Delta} |\tau_{5b}|^{h_k - 1 + 2\Delta} |\tau_{5c}|^{h_k + 1 - 2\Delta}} \Bigg] \,.
\end{aligned} \tag{3.1.9}$$

The integral (3.1.8), can be simplified by the change of variables, $\tau_a \to \tau_1 - (1/\tau_a)$, and $\tau_b \to \tau_1 - (1/\tau_b)$. The simplification is done by first decomposing the integral into sums of integrals. Namely the integration from $-\infty$ to ∞ will be written as a sum of two, an integral from $-\infty$ to 0 and an integral from 0 to ∞. We implement the change of variables on each fragment separately, simplify each of them before recombining them back. At

the end of this exercise, we get

$$I^{(1)}_{nmk}(\tau_1,\tau_3,\tau_5) = \mathrm{sgn}(\tau_{12})\mathrm{sgn}(\tau_{56})\int_{-\infty}^{\infty} d\tau_a\, d\tau_b \left[\frac{1}{|\tau_{31}|^{2h_m}|\tau_{51}|^{2h_k}} \times \frac{|\tau_{ab}|^{h_n+h_m+h_k-2}\mathrm{sgn}(\tau_{51}\tau_a+1)\mathrm{sgn}(\tau_{51}\tau_b+1)}{|\tau_a+\frac{1}{\tau_{31}}|^{h_m}|\tau_b+\frac{1}{\tau_{31}}|^{h_m}|\tau_a+\frac{1}{\tau_{51}}|^{h_k}|\tau_b+\frac{1}{\tau_{51}}|^{h_k}}\right] . \tag{3.1.10}$$

These change of variables are followed up by another pair of change of variables which are carried out in a sequential manner. We will first implement $\tau_a \to \tau_a - (1/\tau_{31})$, and $\tau_b \to \tau_b - (1/\tau_{31})$ and then we will rescale the integration variables $\tau_a \to (\tau_{53}\tau_a)/(\tau_{31}\tau_{51})$ and $\tau_b \to (\tau_{53}\tau_b)/(\tau_{31}\tau_{51})$.

$$I^{(1)}_{nmk}(\tau_1,\tau_3,\tau_5) = \frac{\mathrm{sgn}(\tau_{12})\mathrm{sgn}(\tau_{56})}{|\tau_{31}|^{h_n+h_m-h_k}|\tau_{51}|^{h_n+h_k-h_m}|\tau_{53}|^{h_k+h_m-h_n}} \times \tilde{I}^{(1)}_{nmk}(h_n,h_m,h_k) ,$$

$$\tilde{I}^{(1)}_{nmk}(h_n,h_m,h_k) = \int_{-\infty}^{\infty} d\tau_a\, d\tau_b \frac{|\tau_{ab}|^{h_n+h_m+h_k-2}\mathrm{sgn}(\tau_a-1)\mathrm{sgn}(\tau_b-1)}{|\tau_a|^{h_m}|\tau_b|^{h_m}|1-\tau_a|^{h_k}|1-\tau_b|^{h_k}} = \tilde{S}^{full}_{2,2}(\alpha,\beta,\gamma) , \tag{3.1.11}$$

where, $\alpha = -h_n + 1, \beta = -h_k + 1$, and $\gamma = \frac{h_n+h_m+h_k}{2} - 1$.

As in [48], we divide the Selberg integral, $\tilde{S}^{full}_{2,2}$, into different parts. This is achieved by decomposing the integral into three pieces $[-\infty, 0]$, $[0, 1]$ and $[1, \infty]$ for each integration variable. This results in six Selberg integrals with appropriately modified arguments. Carefully keeping track of the signs, gives

$$\begin{aligned}\tilde{S}^{full}_{2,2}(\alpha,\beta,\gamma) &= S_{2,2}(\alpha,\beta,\gamma) + S_{2,2}(1-\alpha-\beta-2\gamma,\beta,\gamma) \\ &+ S_{2,2}(1-\alpha-\beta-2\gamma,\alpha,\gamma) + 2S_{2,1}(1-\alpha-\beta-2\gamma,\alpha,\gamma) \\ &- 2S_{2,1}(\alpha,\beta,\gamma) - 2S_{2,1}(\alpha,1-\alpha-\beta-2\gamma,\gamma) .\end{aligned} \tag{3.1.12}$$

The generalized Selberg integrals and some important results which are used above are given in [48], but for completeness we give the relevant definitions here

$$\begin{aligned}S_{n,n}(\alpha,\beta,\gamma) &= \int_{[0,1]^n} d\tau_1 ... d\tau_n \prod_{i=1}^{n} |\tau_i|^{\alpha-1}|1-\tau_i|^{\beta} \prod_{i<j} |\tau_{ij}|^{2\gamma} , \\ S_{n,p}(\alpha,\beta,\gamma) &= \int_{[0,1]^p}\int_{[1,\infty)^{n-p}} d\tau_1 ... d\tau_n \prod_{i=1}^{n} |\tau_i|^{\alpha-1}|1-\tau_i|^{\beta} \prod_{i<j} |\tau_{ij}|^{2\gamma} .\end{aligned} \tag{3.1.13}$$

In a similar fashion one can manipulate $I^{(2)}_{nmk}$ to bring it in a form of the conformal three point function. This computation, however, is considerably more involved so we instead do the analysis in the large q. The $I^{(2)}_{nmk}$ in our case differs from that obtained in [48] by only the *sgn* functions while the rest of the integrand has exactly the same form. So for us also at large q, $I^{(2)}_{nmk}$ takes the form,

$$I^{(2)}_{nmk}(\tau_1,\tau_2,\tau_3) \approx \frac{\tilde{s}^{(2)}_{nmk}}{|\tau_{31}|^{h_n+h_m-h_k}|\tau_{51}|^{h_n+h_k-h_m}|\tau_{53}|^{h_k+h_m-h_n}} + \cdots \tag{3.1.14}$$

In our case of course $\tilde{s}^{(2)}_{nmk}$ is different from $s^{(2)}_{nmk}$ obtained by Gross and Rosenhaus [48].

3.2 Away from the Conformal Limit

In this section we carry out the calculation of correlation functions away from the conformal IR fixed point. In the previous chapter we studied the effect of introducing a chemical potential μ, in the SYK-model with complex fermions. We found that a non-zero μ takes us away from the conformal limit since it explicitly introduces a scale in the problem. The effect of introduction of this scale parameter is reflected in the chaotic behavior of the model, namely, it brings down the value of the Lyapunov exponent. We computed the required quantities and studied the maximally chaotic mode(in the large q limit where things can be handled analytically).

We write below the relevant expressions in the large q limit. The two point function(to the leading order in large N) is given by

$$G(\mu,\tau) = G_0(\mu,\tau)\left(1+\frac{1}{q}\log\left(\frac{\cos\left(\frac{\pi\nu}{2}\right)}{\cos\left[\pi\nu\left(\frac{1}{2}-\frac{\tau}{\beta}\right)\right]}\right)+..\right), \tag{3.2.1}$$

where,

$$G_0(\mu,\tau) = -\frac{e^{\mu\tau}}{e^{\mu\beta}+1}, 0\le\tau\le\beta, \tag{3.2.2}$$

$$G_0(\mu,\tau) = \frac{e^{\mu\tau}}{e^{-\mu\beta}+1}, -\beta\le\tau\le 0. \tag{3.2.3}$$

The above relation can be written in a compact manner by,

$$G_0(\mu,\tau) = -sgn(\tau)\frac{e^{\mu\tau}}{e^{\mu\beta sgn(\tau)}+1}, \quad 0\le\tau\le\beta. \tag{3.2.4}$$

We now aim at calculating the enhanced contribution to the four point function slightly away from the conformal limit with the chemical potential μ. Note that since we want to be slightly away from the IR, we will keep $\mu\beta$ to be small and expand all functions in this variable. Then it can be interpreted that we move slightly away from the IR by turning on a small chemical potential.

To this end we need to first calculate the shift in the eigenvalue of the Kernel for the $h=2$ mode. For this we incorporate the technique used in [21]. We begin with the equation,

$$K\Psi = k\Psi, \quad \Rightarrow \quad \int\int K(\tau_1,\tau_2,\tau_3,\tau_4)\Psi(\tau_3,\tau_4)d\tau_3 d\tau_4 = k\Psi(\tau_1,\tau_2). \tag{3.2.5}$$

The Kernel is given by,

$$K(\tau_1,\tau_2,\tau_3,\tau_4) = -(-1)^{q/2}J^2(q-1)G(\mu,\tau_{13})G(\mu,-\tau_{24})G(\mu,\tau_{34})^{q/2-1}G(\mu,-\tau_{34})^{q/2-1}. \tag{3.2.6}$$

We will work in the large q limit. Substituting the Kernel in equation (3.2.5) gives

$$-qJ^2\int d\tau_3 d\tau_4 \frac{sgn(\tau_{13})sgn(\tau_{24})e^{\mu\tau_{13}}e^{-\mu\tau_{24}}}{(e^{\mu\beta sgn(\tau_{13})}+1)(e^{-\mu\beta sgn(\tau_{24})}+1)}\frac{\cos^2\left(\frac{\pi\nu}{2}\right)}{\sin^2\left(\frac{\tilde{x}_{34}}{2}\right)}$$

$$\times \frac{\Psi(\tau_3,\tau_4)}{\{(e^{\mu\beta sgn(\tau_{34})}+1)(e^{-\mu\beta sgn(\tau_{34})}+1)\}^{q/2-1}} = k\Psi(\tau_1,\tau_2)\,, \tag{3.2.7}$$

where ν is defined in (2.1.1) and $\tilde{x}_{ij} = \frac{2\pi\nu\tau_{ij}}{\beta} + \pi(1-\nu)$. Multiplying (3.2.7) by $e^{-\mu\tau_{12}}$ on both sides of the equation, and differentiating twice, once with respect to τ_1 and once with respect to τ_2 gives,

$$\partial_{\tau_1}\partial_{\tau_2}\left(\frac{sgn(\tau_{13})sgn(\tau_{24})}{(e^{\mu\beta sgn(\tau_{13})}+1)(e^{-\mu\beta sgn(\tau_{24})}+1)}\right) = 4\delta(\tau_{13})\delta(\tau_{24})\,. \tag{3.2.8}$$

Using the parametrization $k = \frac{2}{h(h-1)}$ eq.(3.2.7) reduces to,

$$-\frac{qJ^2\cos^2\left(\frac{\pi\nu}{2}\right)}{(2+2\cosh(\mu\beta))^{q/2-1}} \times \frac{e^{-\mu\tau_{12}}}{\sin^2\left(\frac{\tilde{x}_{12}}{2}\right)}\Psi(\tau_1,\tau_2) = \frac{2}{h(h-1)}\partial_{\tau_1}\partial_{\tau_2}\left(e^{-\mu\tau_{12}}\Psi(\tau_1,\tau_2)\right)\,. \tag{3.2.9}$$

If we substitute $\Psi(\tau_1,\tau_2) = e^{\mu\tau_{12}}e^{-in(\tau_1+\tau_2)}\psi_n(\tau_{12})$ then after some manipulation of eq.(3.2.9) (also using (2.1.1)) we arrive at the differential equation,

$$\left[n^2 + 4\partial_x^2 - \frac{\nu^2 h(h-1)}{\sin^2\left(\frac{\tilde{x}}{2}\right)}\right]\psi_n(x) = 0\,. \tag{3.2.10}$$

Here, $x = \frac{2\pi\tau}{\beta}$ and we have suppressed the subscript on τ since everything is now a function of the time difference τ_{12}.

The solution to this equation with appropriate boundary condition is well known. In fact this is the same equation as obtained in [21]. The solution is given by, (with $\tilde{n} = n/\nu$)

$$\begin{aligned}
\psi_{h,n}(x) &= \left(\sin\frac{\tilde{x}}{2}\right)^h {}_2F_1\left(\frac{h-\tilde{n}}{2}, \frac{h+\tilde{n}}{2}, \frac{1}{2}; \cos^2\left(\frac{\tilde{x}}{2}\right)\right), \quad n = \text{even} \\
\psi_{h,n}(x) &= \cos\frac{\tilde{x}}{2}\left(\sin\frac{\tilde{x}}{2}\right)^h {}_2F_1\left(\frac{h-\tilde{n}+1}{2}, \frac{h+\tilde{n}+1}{2}, \frac{3}{2}; \cos^2\left(\frac{\tilde{x}}{2}\right)\right), \; n = \text{odd}\,.
\end{aligned}$$

The quantization condition on h is obtained by demanding that the wave function vanishes at $x = 0$, *i.e.*, $\tilde{x} = \pi(1-\nu)$. As we approach the conformal limit $\nu \to 1$ this solution actually diverges for generic values of h near 2 (we are interested in the $h = 2$ eigenfunctions). But we want values of h such that the solutions are finite or vanishing, so the first or second argument of the hypergeometric has to be a negative integer. This gives the quantization of h near 2 to be,

$$h_n = 2 + |\tilde{n}| - |n|, \quad h_n = 2 + |n|\left(\frac{1-\nu}{\nu}\right)\,. \tag{3.2.11}$$

This gives the shift in the eigenvalue $k = \frac{2}{h(h-1)}$ to be,

$$k(2,n) = 1 - \frac{3|n|}{2}(1-\nu) + \left(\frac{7n^2}{4} - \frac{3|n|}{2}\right)(1-\nu)^2 + \ldots\,. \tag{3.2.12}$$

This result is identical to the shift obtained in [21], only difference being that ν now depends on the effective coupling $\beta\mathcal{J}_{\text{eff}}$ instead of $\beta\mathcal{J}$.

3.2.1 The enhanced four point contribution

Let us now look at the four point function and use the above result to figure out the enhanced contribution for the Schwarzian mode slightly away from the conformal limit. We begin with the expansion of the four point function in the basis of eigenfunctions of the Kernel, (using the variable $\theta = \frac{2\pi\tau}{\beta}$ on the thermal circle and the period becomes 2π)

$$\frac{\mathcal{F}(\theta_1,\theta_2,\theta_3,\theta_4)}{G(\theta_{12})G(\theta_{34})} = 2\sum_{h,n}\frac{k(h,n)}{1-k(h,n)}\Psi^{\text{exact}}_{h,n}(\theta_1,\theta_2)\Psi^{\text{exact}*}_{h,n}(\theta_3,\theta_4)\,. \tag{3.2.13}$$

To find the enhanced contribution of the Schwarzian or $h = 2$ mode we use the eigenfunction of the Casimir for $h = 2$ and the shifted eigenvalue in the denominator. In the numerator we just use the eigenvalue with $h = 2$ in the IR. This is done to ensure that we are only slightly away from the conformal limit driven by introducing a small chemical potential. Here we will use all results for the large q limit,

$$\frac{\mathcal{F}(\theta_1,\theta_2,\theta_3,\theta_4)}{G(\theta_{12})G(\theta_{34})} = \frac{2\beta\mathcal{J}_{\text{eff}}}{\pi^2}\sum_{|n|\geq 2}\frac{e^{in(y'-y)}}{n^2(n^2-1)}\left[\frac{\sin\left(\frac{nx}{2}\right)}{\tan\left(\frac{x}{2}\right)}-n\cos\left(\frac{nx}{2}\right)\right]\left[\frac{\sin\left(\frac{nx'}{2}\right)}{\tan\left(\frac{x'}{2}\right)}-n\cos\left(\frac{nx'}{2}\right)\right]. \tag{3.2.14}$$

Here,

$$x = \theta_1-\theta_2,\quad x' = \theta_3-\theta_4,\quad y = \frac{\theta_1+\theta_2}{2},\quad y' = \frac{\theta_3+\theta_4}{2}\,. \tag{3.2.15}$$

We have used $1-\nu \sim \frac{2}{\beta\mathcal{J}_{\text{eff}}}$ for large $\beta\mathcal{J}_{\text{eff}}$.

We will now carry out the sum over n. The final expression after all simplifications is complicated, and to get some sensible result for the six point function using these results we resort to doing numerical computation. That is, we carry out the integration numerically to see the behavior of the six point function. We also deduce the chaotic behavior of the OTO six point correlator even though we do not have an analytic result.

3.2.2 The "Contact" and and “Planar" diagrams

What we want to now claim is that among the Contact diagrams and Planar diagrams, which contribute to the six point function at leading order in $\sim 1/N$, the contact diagrams dominates the planar ones by an order q^4, for the enhanced non-conformal mode contribution to the four point function. So at large q, the contact ones dominate over the planar ones, and hence we will look at only the former. But let us show a brief argument for why that is true.

The contact contribution goes as,

$$S_c = (q-1)(q-2)J^2\int d\tau_a d\tau_b G(\tau_{ab})^{\frac{q}{2}-3}G(-\tau_{ab})^{\frac{q}{2}}\mathcal{F}(\tau_1,\tau_2,\tau_a,\tau_b)\mathcal{F}(\tau_3,\tau_4,\tau_a,\tau_b)\mathcal{F}(\tau_5,\tau_6,\tau_a,\tau_b)\,. \tag{3.2.16}$$

While the planar contribution goes as,

$$\mathcal{S}_p = \int_{-\infty}^{\infty} d\tau_a d\tau_b d\tau_c \mathcal{F}_{\text{amp}}(\tau_1,\tau_2,\tau_a,\tau_b)\mathcal{F}_{\text{amp}}(\tau_4,\tau_3,\tau_c,\tau_a)\mathcal{F}_{\text{amp}}(\tau_5,\tau_6,\tau_b,\tau_c)\,, \tag{3.2.17}$$

where,

$$\mathcal{F}_{\text{amp}}(\tau_1,\tau_2,\tau_3,\tau_4) = -\int_0^\beta d\tau_0 \mathcal{F}(\tau_1,\tau_2,\tau_3,\tau_0)\int \frac{d\omega_4}{2\pi} e^{-i\omega_4\tau_{40}} \frac{1}{G(\mu,\omega_4)}\,,$$

is the amputated four point function. We can use the SD equations to write,

$$\frac{1}{G(\mu,\omega_4)} = -i\omega_4 + \mu - \Sigma(\mu,\omega_4)\,. \tag{3.2.18}$$

Since we are working at finite temperature, we have to do a Matsubara sum. Notice that the $i\omega + \mu$ term has no poles, so when we evaluate the sum using the contour integration prescription, this part vanishes and we are left with,

$$\begin{aligned}\mathcal{F}_{\text{amp}}(\tau_1,\tau_2,\tau_3,\tau_4) &= \int_0^\beta d\tau_0 \mathcal{F}(\tau_1,\tau_2,\tau_3,\tau_0)\Sigma(\mu,\tau_{40})\,,\\ \mathcal{F}_{\text{amp}}(\tau_1,\tau_2,\tau_3,\tau_4) &= J^2\int_0^\beta d\tau_0 \mathcal{F}(\tau_1,\tau_2,\tau_3,\tau_0)G(\tau_{40})^{q/2-1}G(-\tau_{40})^{q/2}\,.\end{aligned} \tag{3.2.19}$$

Now we can convert the τ integrals to θ integrals via appropriate scaling and we get,

$$S_c \sim \frac{q(\beta\mathcal{J}_{eff})^3}{(2\pi)^2}\,, \tag{3.2.20}$$

where,

$$\mathcal{F}_{\text{amp}}(\tau_1,...,\tau_4) \sim \frac{\beta\mathcal{J}_{eff}}{2\pi q\beta}\,. \tag{3.2.21}$$

In terms of the θ variable we have,

$$\mathcal{F}(\theta_i,\theta_j,\theta_a,\theta_b) \sim \beta\mathcal{J}_{\text{eff}}G(\theta_{ij})G(\theta_{ab})\,, \tag{3.2.22}$$

and in the large q limit, for large but finite $\beta\mathcal{J}_{\text{eff}}$,

$$(G(\theta_{ab}))^{\frac{q}{2}}(G(-\theta_{ab}))^{\frac{q}{2}} \sim \frac{1}{(\beta\mathcal{J}_{\text{eff}})^2\sin^2\left(\frac{\theta_{ab}}{2}\right)}\,. \tag{3.2.23}$$

Here we have put $\nu = 1$ inside the sine function which is consistent to the leading order with $\nu \to 1$ as $\beta\mathcal{J}_{eff} \to \infty$. As a consequence the $(\beta\mathcal{J}_{\text{eff}})^2$ coefficient of the "Contact" diagram as well as the amputated four point function cancels out due to the $(\beta\mathcal{J}_{\text{eff}})^2$ appearing in the denominator of (3.2.23). Now since the planar diagram is given by the product of three amputated four point functions hence, when we take the product and convert the τ integrals to θ integrals in (3.2.17), we finally get,

$$\mathcal{S}_p \sim \frac{(\beta\mathcal{J}_{\text{eff}})^3}{q^3(2\pi)^6}\,. \tag{3.2.24}$$

Taking the ration of S_c with $\mathcal{S}_p$ we see that,

$$\frac{S_c}{\mathcal{S}_p} \sim (2\pi)^4 q^4\,. \tag{3.2.25}$$

So in the large q limit as one can easily see that the contact diagram is far more dominant compared to the planar ones and hence it is justified to consider the contribution of the contact diagrams only.

3.2.3 The six point function

Although one can get an analytic answer for the enhanced four point contribution slightly away from the conformal limit, calculation of the full six point function becomes somewhat messy to carry out analytically. We therefore compute the six point function using numerical methods.

Let us first summarize the results, we will then we state all the relevant values used in carrying out these computations.

- We first compute the six point contribution with three $h = 2$ mode keeping all the time arguments to be separate and then we take the short time limit $\theta_1 \to \theta_2$ or $\theta_3 \to \theta_4$. We see that the six point function decreases in this limit for various small values of $\mu\beta$ keeping $\beta\mathcal{J}$ fixed at some large value.

- We then reverse the order, that is we first take the triple short time limit and then carry out the integrals numerically for all the possible nonconformal contributions, *i.e.*,

$$\mathcal{F}_{h=2}\mathcal{F}_c\mathcal{F}_c, \quad \mathcal{F}_{h=2}\mathcal{F}_{h=2}\mathcal{F}_c, \quad \mathcal{F}_{h=2}\mathcal{F}_{h=2}\mathcal{F}_{h=2}\,. \tag{3.2.26}$$

  We find that among the three terms listed above, the first contribution almost vanishes up to any order in $\mu\beta$ that we are working with, whereas the other two terms are small but are of the same order and they go as $(\mu\beta)^2$ with small coefficients. These will get corrected as we go to higher orders.

- To benchmark the code we compute $\lambda^{(1)}_{11k}$ (as was done in [48] for all three conformal modes) for the contact diagrams and plot it against k, where for large k, $h_k = 2k + 1 + 1/2\Delta + O(1/k)$. We find the similar fall off behavior at large k.

Let us now look at some details of the analysis. One of the things that we have to keep in mind is that we are slightly away from the conformal limit because we have turned on a small $\mu\beta$. We need to be careful while working with the conformal modes. Due to explicit scale in the theory, the modes may not be conformal anymore. In other words, the normalized four point contributions of these modes may not be a function of only the cross ratio χ anymore. However, for small $\beta\mu$, the conformal perturbation theory makes sense and within this limit using the conformal basis is justified.

If we recall the eigenvectors of the Kernel then we see that,

$$\Psi(\theta_1, \theta_2) = e^{\frac{\mu\beta}{2\pi}(\theta_{12})} e^{in\frac{\theta_1+\theta_2}{2}} \psi_n(\theta_{12})\,,$$

and to obtain the conformal modes one has to go to the IR, do the sum over n in the four point function to obtain the sum over integer values of h as well as the integral over the principle continuous series. One then deforms the contour to pick up the poles at $k_c = 1$, eigenvalue of the kernel in the conformal limit. In the IR limit the exponential $\mu\beta$ factor becomes equal to 1, but since it has no n dependence it plays no role when we carry out the sum over n. Therefore, slightly away from the conformal limit we will have (small

$\mu\beta$),

$$\frac{\mathcal{F}_{h\neq 2}(\theta_1,\theta_2,\theta_3,\theta_4)}{G(\theta_{12})G(\theta_{34})} = e^{\frac{\mu\beta}{2\pi}(\theta_{12}+\theta_{34})}\sum_{m=1}^{\infty} c_m^2 \chi^{h_m}\, {}_2F_1(h_m,h_m,2h_m,\chi) \quad (3.2.27)$$

$$= \sum_{m=1}^{\infty} c_m^2 \chi^{h_m}\, {}_2F_1(h_m,h_m,2h_m,\chi) + \frac{\mu\beta(\theta_{12}+\theta_{34})}{2\pi}\sum_{m=1}^{\infty} c_m^2 \chi^{h_m}\, {}_2F_1(h_m,h_m,2h_m,\chi)$$

$$+\left(\frac{\mu\beta}{2\pi}\right)^2 \frac{(\theta_{12}+\theta_{34})^2}{2!} \sum_{m=1}^{\infty} c_m^2 \chi^{h_m}\, {}_2F_1(h_m,h_m,2h_m,\chi) + \cdots .$$

The above expression breaks conformal invariance and this is the four point function we will be working with away from the conformal limit.

Since $\beta\mathcal{J}_{\text{eff}}$ appears as an overall factor we strip of this factor and look at the integrals only. For small $\mu\beta$ this factor is large but finite. $\mu\beta$ is kept to be $\sim 7.4\times 10^{-4}$.

3.2.4 The Short time and OTO behavior of the Six point function

Since this is a part of the non-conformal piece, we will first compute it by keeping all times different and then taking one time approaching another for example $\tau_1 \to \tau_2$, and look at how it behaves. In Figure 3.1, we see the behavior of the six point as we take the short time limit. It is easy to check that when we compute the six point function in the triple short time limit vanishes.

The contribution to the non-conformal piece coming from the product of three $h = 2$ modes is shown in Fig. 3.1. In computing the contribution for one or two $h \neq 2$ modes,

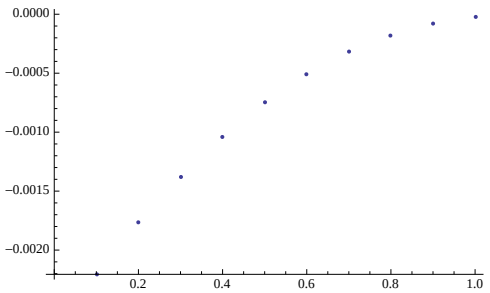

Figure 3.1: The plot of the six point function vs τ_1 as $\tau_1 \to \tau_2$.

we have to be careful as what happens to the “Planar" diagrams as well. For more details see, Appendix A.

For calculating the OTO correlation function we have to first set a specific configuration of operators, which is then analytically continued to real time. However, we do not have the analytic expression so we use the following procedure. We modify the times that are to be analytically continued keeping their relative positions to be the same. This effectively corresponds to changing only one time independently. We observe the behavior of the correlator and compare it with the behavior of the enhanced four point function (for which

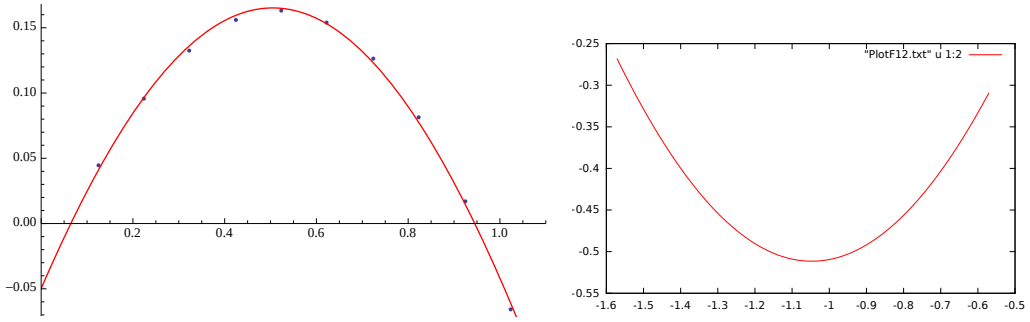

Figure 3.2: The OTO six point and four point function response for changing τ_1.

we already know that there is a chaotic behavior) under the same operation. From the results plotted in fig. 3.1 and fig. 3.2 above it is easy to see that the six point OTO correlation function actually does exhibit chaotic behavior when we analytically continue to real time. The chaos exponent can be estimated by fitting the data with an oscillatory function. We choose an ansatz

$$a + b\sin(\lambda\tau) + c\cos(\lambda\tau)\,. \tag{3.2.28}$$

We find that the data is fitted for the following values of a, b, c, and λ,

$$\begin{aligned} a &= -0.68904\,, \\ b &= 0.56662\,, \\ c &= 0.63927\,, \\ \lambda &= 1.4364\,. \end{aligned} \tag{3.2.29}$$

The maximal value of the Lyapunov is $3/2$ but the fitted value of λ is less than the maximal. This is due to the errors in our numerical computation. Because of the small but non-vanishing value of the chemical potential μ we are indeed slightly away from the conformal limit but since we are working with the enhanced contribution we should have gotten a value which is nearer to $3/2$. Here we would like to mention that, upto these errors, this value of λ is in agreement with [62], as the maximal chaos exponent for the six point OTOC.

3.3 Appendix A

If we consider the behavior of $\mathcal{F}_{\text{amp}}$ for the $h = 2$ mode as we take two times to be closer to each other, then we find the results shown in Figure 3 below.
As we can see from the graph the value of $\mathcal{F}_{\text{amp}}$ is quite large when the times are well separated. But computing the six point “Planar" diagram in the triple short time limit numerically one finds that the contribution is small i.e of the same order as the “Contact" integrals hence using the fact that the coefficient of the “Contact" diagrams are much

dominant over the “Planar" ones, we are justified in considering the contribution of the former only. Although one has to be careful when considering the “Planar" contribution when $h \neq 2$ modes are taken but since the numerics is pretty involved and takes very long time we do not present those results here.

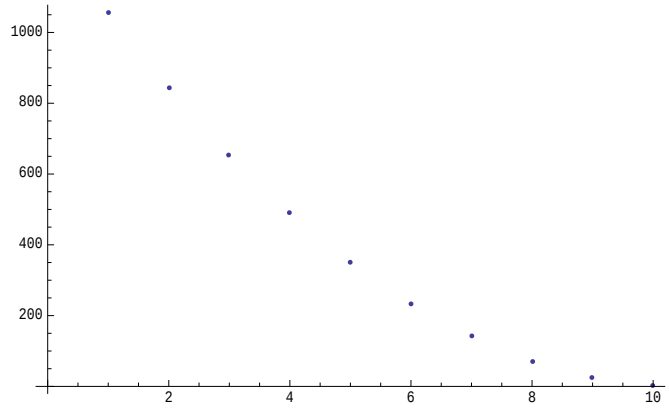

Figure 3.3: Plot of $\mathcal{F}_{\text{amp}}$ against θ_1 as it is taken towards to θ_2. Along the θ_1 axis we mark the number of steps while the actual interval is $0 - 1$ in steps of 0.1.

3.4 Appendix B

In this appendix we collect the expressions of the constants that appear in six point amplitude.

$$c_n = \frac{2q}{(q-1)(q-2)\tan(\pi\Delta)} \frac{(h_n - \frac{1}{2})}{\tan\left(\frac{\pi h_n}{2}\right)} \frac{\Gamma^2(h_n)}{k'_A(h_n)\Gamma(2h_n)}\,, \tag{3.4.1}$$

$$\tilde{c}_n = \frac{2q}{(q-1)(q-2)\tan(\pi\Delta)} \frac{(h_n - \frac{1}{2})}{\cot\left(\frac{\pi h_n}{2}\right)} \frac{\Gamma^2(h_n)}{k'_S(h_n)\Gamma(2h_n)}\,, \tag{3.4.2}$$

$$\xi_n = b^q \pi^{1/2} \frac{\Gamma(1-\Delta+\frac{h_n}{2})\Gamma(\frac{1}{2}-\frac{h_n}{2})\Gamma(\Delta)}{\Gamma(\frac{1}{2}+\Delta-\frac{h_n}{2})\Gamma(\frac{h_n}{2})\Gamma(\frac{3}{2}-\Delta)}\,, \tag{3.4.3}$$

$$\tilde{\xi}_n = b^q \pi^{1/2} \frac{\Gamma(\frac{1}{2}-\Delta+\frac{h_n}{2})\Gamma(1-\frac{h_n}{2})\Gamma(\Delta)}{\Gamma(\Delta-\frac{h_n}{2})\Gamma(\frac{1}{2}+\frac{h_n}{2})\Gamma(\frac{3}{2}-\Delta)}\,. \tag{3.4.4}$$

4 Thermalization in the SYK model

Here we study non-equilibrium dynamics in SYK models using quantum quench. We consider models with two, four, and higher fermion interactions ($q = 2, 4$, and higher) and use two different types of quench protocol, which we call step and bump quenches. We analyse evolution of fermion two-point functions without long time averaging. We observe that in $q = 2$ theory the two-point functions do not thermalize. We find thermalization in $q = 4$ and higher theories without long time averaging. We also calculate two different exponents of which one is equal to the coupling and the other is proportional to the final temperature. This result is more robust than thermalization obtained from long time averaging as proposed by the eigenstate thermalization hypothesis(ETH). Thermalization achieved without long time averaging is more akin to mixing than ergodicity.
Our main object of interest is the Kadanoff-Baym equations which we will use to analyse the non-equilibrium dynamics of the SYK model. Before we set up the Kadanoff-Baym equations, let us consider the Schwinger-Dyson equation.

4.1 Why non-equilibrium dynamics?

The study of non-equilibrium dynamics is becoming important both in condensed matter physics [43, 50, 63–70] as well as in string theory [20, 45, 71–74]. Applications to holography i.e. in case of a black hole collapse where the system tends towards equilibriation [75, 76] has been in the literature in the recent past. Studies of holographic entanglement entropy, in context of time evolution [77] and multi-scale renormalization ansatz [78–80] is another related area of research which finds the use of non-equilibrium dynamics. One of the most interesting question in this field is to understand patterns of thermalization in the systems which are out of equilibrium. For example, it is important to know under what conditions a closed quantum system thermalizes, i.e., for a system prepared in a pure excited state, and undergoes unitary evolution, determine how the late time limit of the expectation values of certain observables are effectively described by a thermal ensemble[1]. Interest in the non-equilibrium dynamics from string theory point-of-view stems from black hole physics. The AdS/CFT correspondence(or the holographic

[1]The expectation values can equilibrate but the stationary limits may not be described by a thermal ensemble, which we will observe below for $q = 2$ theory for which the fermion two-point functions freeze instantaneously but its values are not described by a thermal ensemble.

principle, in general) says that a black hole corresponds to thermal ensemble in the *boundary* quantum theory, and the thermalization process in the quantum system is conjectured to be dual to black hole formation in the bulk gravitation theory.

On the bulk gravity side it has been conjectured that black holes are fast scramblers [15]. This proposal led to another conjecture [11] that the chaotic behaviour, that leads to scrambling, which is parametrized by the Lyapunov exponent λ_L has an upper bound, and that upper bound is saturated by black holes. This naturally gave additional impetus to the study of non-equilibrium dynamics in systems which exhibit chaos, especially if the Lyapunov exponent of the theory saturates the upper bound.

The eigenstate thermalization hypothesis (ETH) is an attempt to explain how closed unitary quantum systems in pure excited states can thermalize [81, 82]. Thermalization with ETH crucially involves long time averaging of the observables under consideration. It is, however, not clear what is the precise relation between chaos and ETH. In many studies of quantum systems, thermalization is observed even without long-time averaging [65]. Thermalization has also been seen in the integrable systems without long time averaging. The late time behaviour of integrable models is described by the generalized Gibbs ensembles [44, 83]. These ensembles have fugacities turned on for several conserved charges of the integrable system. The integrable model, by definition, is not chaotic on its own.

The most convenient method for studying non-equilibrium dynamics, both theoretically [43, 45, 66–69, 72, 84–86] and experimentally [87, 88], turns out to be quantum quench. In other words, quantum quenches are the most convenient way of generating non-trivial excited states of the theory. In quantum quench one abruptly changes parameters of the Hamiltonian of the system starting from an equilibrium configuration(generally a thermal state or the ground state) of the system. The change in the coupling generally excites the system and the system evolves non-trivially with the final Hamiltonian. The evolution of the system is examined by calculating the expectation values of some of the observables of the system. If the expectation values of those observables approach the expectation values in a thermal ensemble, the system is said to have thermalized.

An important aspect of the work presented in this chapter is to check if step quenches produce special fine-tuned pure states which looks exactly thermal. These pure states are inspired by the Euclidean evolved boundary states of Calabrese and Cardy [89]. These states, which we will refer to as Kourkoulou-Maldacena (KM) states below, have interesting bulk duals [90]. The details of these pure states can be found in section 4.3.2. We observed that the final states of quantum quenches using disordered couplings are not KM states. But one can use mass like terms to perform the sudden step quenches for which the final states are the KM states.

The thermalization we observe in $q = 4$ theory without long time averaging, is much more robust than what one expects from the ETH. We therefore believe that *thermalization in a chaotic system is more akin to mixing in classical systems which is a stronger condition than ergodicity.*

The outline of this chapter is as follows: In section 4.2, we will briefly recall the derivation of the Schwinger-Dyson equation in the SYK model with Majorana fermions. This will also be used to fix our notation. We will write down the Schwinger-Dyson equation for

a model with both $q = 2$ and 4 interactions. The couplings for these terms will have arbitrary time dependence to start with. In section 4.3 we will set up the Kadanoff-Baym equations for this system which can be easily generalized for higher q models. Finally we will briefly discuss the eigenstate thermalization hypothesis(ETH). In section 4.3.2, we discuss Kourkoulou-Maldacena states with an eye on possible relation between our results and these excited states. In section 4.4, we discuss various quench protocols that we study in the SYK model and present results of our numerical computations. Section 5.3 contains conclusion and discussion where we wrap up our results and discuss about ways to prepare Kourkoulou-Maldacena states and the implications of thermalization without long-time averaging.

4.2 The Schwinger-Dyson(SD) equations

We will consider the time dependent Hamiltonian which describes different quench protocols depending on the kind of time dependence we allow for the couplings of the theory. To simplify the matter we will extract the time dependence of the couplings and write it in terms of separate functions of time. For example, up to the quartic fermion interaction *i.e.*, $q = 4$, the Hamiltonian is

$$H(t) = i\sum_{i<j} J_{2,ij} f_2(t)\psi_i\psi_j - \sum_{i<j<k<l} J_{4,ijkl} f_4(t)\psi_i\psi_j\psi_k\psi_l \,, \tag{4.2.1}$$

where, $f_2(t)$ and $f_4(t)$ contain the time dependence of the couplings. The partition function of this model is written in terms of the action functional,

$$S[\psi] = \int_C dt \left\{ \frac{i}{2}\sum_i \psi_i\partial_t\psi_i - i\sum_{i<j} J_{2,ij} f_2(t)\psi_i\psi_j + \sum_{i<j<k<l} J_{4,ijkl} f_4(t)\psi_i\psi_j\psi_k\psi_l \right\} . \tag{4.2.2}$$

All the interaction terms in the SYK model couple all fermions to each other and have random couplings. The randomness of the coupling is meant to mimic the disorder in the system. We will average the partition function over the gaussian distributed random couplings,

$$Z = \int \mathcal{D}\psi \int \mathcal{D}J_{2,ij} \int \mathcal{D}J_{4,ijkl}\, \mathcal{P}_1(J_{2,ij})\mathcal{P}_2(J_{4,ijkl}) \exp(iS[\psi]) \,, \tag{4.2.3}$$

where the gaussian weight functions, $\mathcal{P}_1(J_{2,ij})$ for the quadratic coupling and $\mathcal{P}_2(J_{4,ijkl})$ for the quartic coupling have width $2J_2^2/N$ and $12J_4^2/N$ respectively. Usually in the quenched disorder the integration over the random variables is carried out at the end of the computation, however, in the large N limit we can reverse the order. Carrying out the gaussian integral over the quadratic and quartic couplings gives us the effective action

$$\begin{aligned} iS_{\text{eff}} = &-\int_C dt \frac{1}{2}\sum_i \psi_i\partial_t\psi_i - \frac{1}{2}\times\frac{J_2^2}{2N}\int dt_1 dt_2 \sum_{i,j} f_2(t_1)f_2(t_2)\psi_i(t_1)\psi_i(t_2)\psi_j(t_1)\psi_j(t_2) \\ &+ \frac{3J_4^2}{4!N^3}\int dt_1 dt_2 \sum_{i,j,k,l} f_4(t_1)f_4(t_2)\psi_i(t_1)\psi_i(t_2)\psi_j(t_1)\psi_j(t_2)\psi_k(t_1)\psi_k(t_2)\psi_l(t_1)\psi_l(t_2) \,. \end{aligned} \tag{4.2.4}$$

In this effective action the sum runs over all values of i, j, k, l and the combinatoric factors take care of the ordering of fermions in each term. Following [43], we will write this effective action in terms of auxiliary fields and convert it into a quadratic action in terms of the fermions. The path integral in terms of the auxiliary functions, suggestively named as $G(t)$ and $\Sigma(t)$,

$$\begin{aligned} Z = \int \mathcal{D}\psi\, \mathcal{D}G\, \mathcal{D}\Sigma\, \exp\Bigg[& -\int_C dt \frac{1}{2}\sum_i \psi^i \partial_t \psi^i + \frac{J_2^2 N}{4}\int_C dt_1 dt_2 f_2(t_1) f_2(t_2) G(t_1,t_2)^2 \\ & -\frac{3J_4^2 N}{4!}\int_C dt_1 dt_2 f_4(t_1) f_4(t_2) G(t_1,t_2)^4 \\ & +\frac{i}{2}\int_C dt_1 dt_2 \Sigma(t_1,t_2)\left(G(t_1,t_2) + \frac{i}{N}\sum_i \psi_i(t_1)\psi_i(t_2)\right)\Bigg] , \end{aligned} \tag{4.2.5}$$

where,

$$G(t_1,t_2) = -\frac{i}{N}\sum_i \psi_i(t_1)\psi_i(t_2) . \tag{4.2.6}$$

The auxiliary field Σ is introduced so that we can implement the constraint (4.2.6) as an equation of motion of Σ. This is done by implementing the constraint through the δ-function. This procedure reduces the action (4.2.5) to quadratic form in terms of the fermions. We can now integrate out the Majorana fermions and write the effective action $S[G,\Sigma]$ purely in terms of G and Σ,

$$\begin{aligned} S[G,\Sigma] = & -\frac{iN}{2}\mathrm{Tr}(\log\left[-i(G_0^{-1} - \Sigma)\right]) + \frac{iJ_2^2 N}{4}\int dt_1 \int dt_2 f_2(t_1) f_2(t_2) G(t_1,t_2)^2 \\ & - \frac{3iJ_4^2 N}{4!}\int dt_1 \int dt_2 f_4(t_1) f_4(t_2) G(t_1,t_2)^4 + \frac{iN}{2}\int dt_1 dt_2 \Sigma(t_1,t_2) G(t_1,t_2) . \end{aligned} \tag{4.2.7}$$

An advantage of this form of the effective action is that the Schwinger-Dyson equations can be derived as equations of motion of this action,

$$\Sigma(t_1,t_2) = G_0^{-1}(t_1,t_2) + G^{-1}(t_1,t_2) , \tag{4.2.8}$$

$$\Sigma(t_1,t_2) = J_2^2 f_2(t_1) f_2(t_2) G(t_1,t_2) - J_4^2 f_4(t_1) f_4(t_2) G(t_1,t_2)^3 . \tag{4.2.9}$$

A similar analysis can be carried out for the six and higher fermion interactions in an analogous manner. Let us now consider the eq.(4.2.9) and take the convolution product with $G(t_1,t_2)$ from both right and left, this procedure gives us two equation,

$$\int_C dt_3 G_0^{-1}(t_1,t_3) G(t_3,t_2) = \delta_C(t_1,t_2) + \int_C dt_3 \Sigma(t_1,t_3) G(t_3,t_2) , \tag{4.2.10}$$

$$\int_C dt_3 G(t_1,t_3) G_0^{-1}(t_3,t_2) = \delta_C(t_1,t_2) + \int_C dt_3 G(t_3,t_2) \Sigma(t_1,t_3) . \tag{4.2.11}$$

To study the Kadanoff-Baym equations besides eq. (4.2.10), (4.2.11) we will need the retarded, the advanced and the Keldysh Green's functions which are defined as

$$G^R(t_1,t_2) \equiv \Theta(t_1 - t_2)[G^>(t_1,t_2) - G^<(t_1,t_2)], \tag{4.2.12}$$

$$G^A(t_1,t_2) \equiv \Theta(t_2-t_1)[G^<(t_1,t_2)-G^>(t_1,t_2)]\,, \tag{4.2.13}$$
$$G^K(t_1,t_2) \equiv G^>(t_1,t_2)+G^<(t_1,t_2)\,. \tag{4.2.14}$$

Along these lines define the retarded, advanced self-energy in the following manner.

$$\Sigma^R(t_1,t_2) \equiv \Theta(t_1-t_2)[\Sigma^>(t_1,t_2)-\Sigma^<(t_1,t_2)]\,, \tag{4.2.15}$$
$$\Sigma^A(t_1,t_2) \equiv -\Theta(t_2-t_1)[\Sigma^>(t_1,t_2)-\Sigma^<(t_1,t_2)]\,. \tag{4.2.16}$$

4.3 The Kadanoff-Baym (KB) equations

Equations (4.2.10) and (4.2.11) can be manipulated using the real space representation of G_0^{-1} on the left hand side and contour deformation on the right hand side to write

$$i\partial_{t_1}G^>(t_1,t_2) = \int_{-\infty}^{\infty} dt_3\{\Sigma^R(t_1,t_3)G^>(t_3,t_2)+\Sigma^>(t_1,t_3)G^A(t_3,t_2)\}\,. \tag{4.3.1}$$

$$-i\partial_{t_2}G^>(t_1,t_2) = \int_{-\infty}^{\infty} dt_3\{G^R(t_1,t_3)\Sigma^>(t_3,t_2)+G^>(t_1,t_3)\Sigma^A(t_3,t_2)\}\,. \tag{4.3.2}$$

Note that the contour starts from some time t_0 and the operators are inserted in the correct order for different values of t_1 and t_2 and then comes back to t_0. For quenches starting from a thermal state, the contour further goes down in the imaginary time direction for an interval of length β_i which is the inverse temperature of the initial thermal state (Figure 4.1).

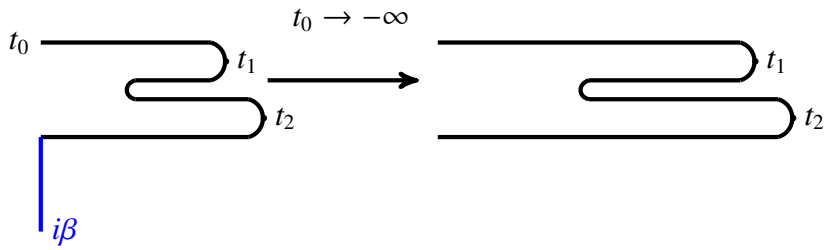

Figure 4.1: Contour deformation for Bogoliubov principle of weakening correlations.

If one takes the limit $t_0 \to -\infty$ then for all observables at finite time, the contribution from the imaginary time interval can be neglected which follows from the Bogoliubov principle of weakening correlations [91].[2]

We will briefly explain derivation of (4.3.1) using the Langreth rules below. Derivation of (4.3.2) follows in an analogous manner. The left hand side of (4.3.1) can be derived starting from the equation(4.2.10), and choosing the Green's function $G(t_3,t_2)$ to be the

[2]For this work, the calculation is further simplified because the free part of the Hamiltonian is zero.

greater Green's function $G^{>}(t_3, t_2)$, and integrating by parts to get

$$\begin{aligned} \text{L.H.S.} &= i \int_C dt_3 (\partial_{t_1} \delta_C(t_1, t_3)) G^{>}(t_3, t_2) \\ &= i \int_C dt_3 \delta_C(t_1, t_3) \partial_{t_3} G^{>}(t_3, t_2) \\ &= i \partial_{t_1} G^{>}(t_1, t_2) \,, \end{aligned} \tag{4.3.3}$$

where we have used the fact that G_0^{-1} is given by the derivative of the δ-function. The right hand side of (4.2.10) is

$$\text{R.H.S.} = \int_C dt_3 \Sigma(t_1^+, t_3) G(t_3, t_2^+) \,. \tag{4.3.4}$$

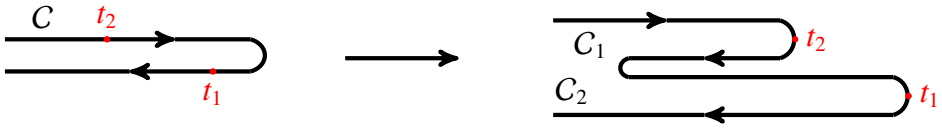

Figure 4.2: Contour deformation for Langreth Rules.

Using the contour deformation we can rewrite (4.3.4) as

$$\int_C dt_3 \Sigma(t_1^+, t_3) G(t_3, t_2^+) = \int_{C_1} d\tau \Sigma(t_1, \tau) G^{>}(\tau, t_2) + \int_{C_2} dt \Sigma^{>}(t_1, t) G(t, t_2) \,. \tag{4.3.5}$$

The first term in (4.3.5) can be written as

$$\begin{aligned} \int_{C_1} d\tau \Sigma(t_1, \tau) G^{>}(\tau, t_2) &= \int_{-\infty}^{t_1} d\tau \Sigma^{>}(t_1, \tau) G^{>}(\tau, t_2) + \int_{t_1}^{-\infty} d\tau \Sigma^{<}(t_1, \tau) G^{>}(\tau, t_2) \\ &= \int_{-\infty}^{\infty} d\tau \Theta(t_1 - \tau) \Sigma^{>}(t_1, \tau) G^{>}(\tau, t_2) - \int_0^{\infty} d\tilde{\tau} \Sigma^{<}(t_1, \tilde{\tau}) G^{>}(\tilde{\tau}, t_2) \,, \end{aligned} \tag{4.3.6}$$

where, $\tilde{\tau} = t_1 - \tau$. Inserting Heaviside $\Theta(\tilde{\tau})$ function in the term involving $\Sigma^{<}$ we can extend the integration limit from $(0, \infty)$ to $(-\infty, \infty)$. After substituting $\tilde{\tau} = t_1 - \tau$, the integral remains invariant. So we get,

$$\begin{aligned} \int_{C_1} d\tau \Sigma(t_1, \tau) G^{>}(\tau, t_2) &= \int_{-\infty}^{\infty} d\tau \Theta(t_1 - \tau) \left(\Sigma^{>}(t_1, \tau) - \Sigma^{<}(t_1, \tau) \right) G^{>}(\tau, t_2) \,, \\ \int_{C_1} d\tau \Sigma(t_1, \tau) G^{>}(\tau, t_2) &= \int_{-\infty}^{\infty} d\tau \Sigma^{R}(t_1, \tau) G^{>}(\tau, t_2) \,. \end{aligned} \tag{4.3.7}$$

Similar manipulations can be carried out for the second term in (4.3.5) to get,

$$\int_{C_2} dt \Sigma^{>}(t_1, t) G(t, t_2) = \int_{-\infty}^{\infty} dt \Sigma^{>}(t_1, t) G^{A}(t, t_2) \,. \tag{4.3.8}$$

4.3.1 Eigenstate Thermalization Hypothesis

It has been shown that the $q = 4$ SYK model with Majorana fermions [70, 74] and complex fermions [20] with large but finite N satisfy the eigenstate thermalization hypothesis (ETH). Although it has been claimed [92] that $q = 2$ SYK model with complex fermions satisfies ETH, it was later found that the finite N scaling in $q = 2$ SYK model with Majorana fermions does not scale correctly with the system size [70]. It has therefore been suggested that $q = 4$ SYK model should thermalize while the $q = 2$ model should not. Our results do not conflict with this suggestion, however, note that ETH necessarily involves long-time averaging of the observables [81, 82, 93]. Long time averaging is not necessary for thermalization or equilibration in many scenario of quantum quenches [65], even in free theories [45]. In fact, it is not even clear what is the relation of ETH with such thermalization or equilibration processes which do not involve long-time averaging after quantum quenches. Also note that in black hole collapse geometries [46, 47, 94], there is no long-time averaging invloved. These geometries are the bulk duals of thermalization in the corresponding boundary CFT.

4.3.2 Kourkoulou-Maldacena states and Instantaneous thermalization

In this section we will introduce certain pure excited states in SYK models. The motivation for constructing these states comes from the boundary state ansatz of quantum quenches in 1D systems in the thermodynamic limit [89]. The ansatz by Calabrese and Cardy corresponds to starting from the ground state of a gapped theory and quenching it to a gapless theory (1+1D CFT), the final state obtained after the quench has the generic form

$$|CC\rangle = e^{-\kappa H_{CFT}}|B\rangle \,, \tag{4.3.9}$$

where $\kappa > 0$ is a parameter fixed by the quench process, H_{CFT} is the Hamiltonian of the final gapless theory and $|B\rangle$ is a conformally invariant boundary state (B state) of the CFT. We will refer to these states as Calabrese-Cardy(CC) states. Determination of the particular B state that is relevant for the description of the post quench state of the system for a specific quantum quench is a non-trivial problem [95]. Nevertheless, using conformal symmetry of the final theory, it can be shown that expectation values of one-point and two-point functions effectively thermalize, where the expectation values in the long-time limit are described by a thermal ensemble with inverse temperature $\beta = 4\kappa$. In fact, it has been shown that finite subsystems thermalize where again the long-time limit is described by a thermal ensemble with inverse temperature $\beta = 4\kappa$ [67, 71]. Since the quench process started from the ground state, the system always remains in a pure state. An interesting aspect of this process of thermalization of subsystems is that correlation functions of holomorphic operators of the final CFT thermalize instantaneously [45, 96].

We will now consider certain pure excited states in SYK models. These states were first constructed by Kourkoulou and Maldacena in [90]. Considering N majorana fermions, the analogous B states are defined as

$$(\psi^{2k-1} - is_k\psi^{2k})|B_s\rangle = 0, \qquad s_k = \pm 1, \qquad k = 1, ..., N/2 \,. \tag{4.3.10}$$

Hence, there are $2^{N/2}$ number of such B states. These are high energy states. One can produce lower energy states by evolving these B states for a finite euclidean time κ. We will refer to these low energy states as KM states.

$$|KM\rangle = e^{-\kappa H}|B_s\rangle \, . \tag{4.3.11}$$

An interesting feature of KM states is that, in the large N limit, "diagonal" two-point functions $\psi^i(t_1)\psi^i(t_2)$ are "instantaneously thermalized"(using the 1+1D CFT terminology used above)

$$\langle KM|\psi^i(t_1)\psi^i(t_2)|KM\rangle = \mathrm{Tr}\left[e^{-\beta H}\psi^i(t_1)\psi^i(t_2)\right], \qquad i = 1, ..., N \to \infty \tag{4.3.12}$$

where the effective inverse temperature $\beta = 2\kappa$. The "off-diagonal" two-point functions $\psi^{2k-1}(t_1)\psi^{2k}(t_2)$ have non-trivial time dependence and decay to zero in the long-time limit. These "off-diagonal" two-point functions are zero in a thermal ensemble. The KM states also have interesting bulk duals in AdS_2.

Unlike in 2D CFT quenches, we could not find any quench scenario with disordered couplings where the final state is the KM state. This work was initially inspired by our curiosity about the possibility of the KM states being the final states of step quenches but not for bump quenches in SYK models. The negative result that the final states in quenches in SYK models are not KM states leads to deeper understanding of the thermalization process in chaotic theories. We will comment further on this issue in the concluding section 5.3.

4.4 Quantum Quenches in SYK models

The KB equations are solved numerically after discretizing the two time arguments t_1 and t_2. For quenches in $q = 2$ theory, we could start from the ground state, since the Green's function oscillates and decays fast with time. For all other cases, we start with a thermal state which gives an exponential decay of the initial data as a function of the relative time difference. Moreover, since we start from a stationary state, all the initial data in the third quadrant are shifted functions of the data on ($t_1 < 0$, $t_2 = 0$) line and ($t_1 = 0$, $t_2 < 0$) line. We use a grid of the kind bounded by red coloured lines in figure 4.3. Since the terms far away from the diagonal fall of exponentially fast, the grid points in the second and fourth quadrant lying outside the red coloured lines are ignored in our numerical code.

We used grids of three different sizes 2001×1001, 3001×1501 and 4001×2001 points. The computation time grows very fast with increasing grid size. We also used a fixed time step size $dt = 0.05$.[3] In the rest of the paper, we will suppress factors of this time step size dt. So, unless it is explicitly mentioned all the times are measured in units of dt. In step protocols, the quenches happen at $t_1 = 0$ and $t_2 = 0$. For all the cases with bump protocol,

[3] We also checked our results with $dt = 0.025$ to make sure some of our results are not due to finite size numerical time steps. But we will not present any numerical results of the runs with $dt = 0.025$. So, $dt = 0.05$ for the rest of the paper.

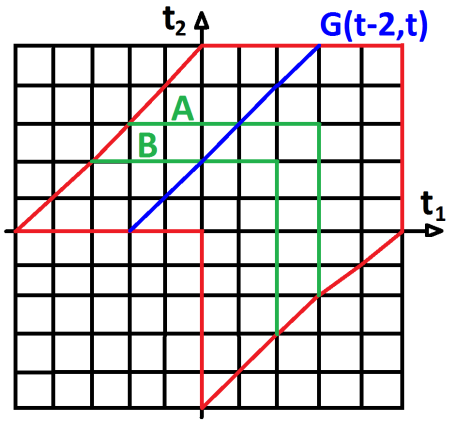

Figure 4.3: The red lines mark the grid used for solving the Kadanoff-Baym equations. This corresponds to ignoring terms on the top left of the second quadrant and the bottom right of the fourth quadrant where the values of $G^{>}(t_1, t_2)$ are negligible.

the perturbations[4] are turned on between $t_1 = 1$ and $t_1 = 10$, similarly between $t_2 = 1$ and $t_2 = 10$ for the other direction. The KB equations are solved self-consistently in this grid using the Predictor-Corrector method. The predicted values on line A are calculated *causally* from the data on line B as shown in figure 4.3. The predicted values are then corrected until the desired accuracy is obtained.

For most of quenches we are considering here, the initial data is obtained by solving the SD equation numerically for finite inverse temperature β [43]. For step quenches in $q = 2$ theory in which J_2 interaction is dominant, we can start from the ground state. The initial data are obtained by solving the SD equation in the ground state ($\beta \to \infty$) numerically. In this case we use

$$\lim_{\beta\to\infty} \frac{1}{1+e^{-\beta\omega}} = \Theta(\omega) = \begin{cases} 0, & \text{if} \quad \omega < 0. \\ 1/2, & \text{if} \quad \omega = 0. \\ 1, & \text{if} \quad \omega > 0. \end{cases} \tag{4.4.1}$$

In case of the bump quench in $q = 2$ theory, for cases in which we start from the ground state, the initial data is calculated using the analytic expression for $G^{>}(t_1, t_2)$. The greater Green's function in ground state for $q = 2$ theory is

$$G^{>}(t_1, t_2) = \frac{1}{2J_2(t_1 - t_2)} \left[J_1(2J_2(t_1 - t_2)) - iH_1(2J_2(t_1 - t_2)) \right] . \tag{4.4.2}$$

Calculation of final temperature: The temperature in the long time limit is calculated using the relation [43]

$$\frac{iG^K(\omega)}{A(\omega)} = \tanh\left(\frac{\beta\omega}{2}\right) , \tag{4.4.3}$$

[4]Note that we are not doing any perturbative or series expansion in our calculation. The word 'perturbation' in this context means exciting the system by turning on the source term which injects energy in the system.

where $G^K(\omega)$ is the Fourier transform of the Keldysh Green's function $G^K(t_1, t_2)$ (4.2.14) which is a function of only $t_1 - t_2$ in a thermal ensemble and $A(\omega)$ is

$$A(\omega) = -2\,\mathrm{Im}\,G^R(\omega)\,. \tag{4.4.4}$$

$G^R(\omega)$ is the Fourier transform of the retarded Green's function $G^R(t_1, t_2)$ (4.2.12) which also is a function of only $t_1 - t_2$ in a thermal ensemble.

The relation (4.4.3) is a result of the KMS condition which ensures [97] that

$$G^>(\omega) = -e^{\beta\omega} G^<(\omega)\,, \tag{4.4.5}$$

and it holds for all fermionic theories. We can therefore conclude that the system under consideration has thermalized only if the quantity on the LHS of (4.4.3) has tanh profile as a function of the frequency ω. Note that for the determination of the final temperature we also have to use the relation between greater and lesser Green's functions (1.1.9).

Check for energy conservation: We also check for energy conservation to ensure that our numerical results are correct. From (4.2.7), the total energy as a function of time t_1 is given by

$$\begin{aligned} E(t_1) &= \int_C dt_2 \Sigma(t_1, t_2) G(t_1, t_2) \\ &= \int_{-\infty}^{t_1} dt_2 \left(\Sigma^>(t_1, t_2) G^>(t_1, t_2) - \Sigma^>(t_2, t_1) G^>(t_2, t_1)\right)\,. \end{aligned} \tag{4.4.6}$$

In the second line, the first term arises from the upper half of the contour and the second term arises from the lower half of the contour. We have also used (1.1.9) for the second term.

The quench processes we are considering, merely satisfying (4.4.3) in the long time limit is not sufficient to guarantee thermalization. This is because, as we mentioned above, all fermionic theories at finite temperature satisfy the relation (4.4.3). So, to check thermalization, we first calculate the final temperature using the above relation. The SD equation of the final theory is then solved at the calculated final temperature and in the end we check if the generated real time two-point functions agree with the two-point functions obtained from the quench process.

4.4.1 Quenches in $q = 2$ SYK model

In this subsection we will study quantum quenches in which the final theory is the $q = 2$ SYK model, that is the model which only has 1-body (quadratic, J_2) interaction. These quenches are special cases because the two-point functions equilibrate instanteneously. From (4.3.1, 4.3.2), for $q = 2$ final theory,

$$\partial_{t_1} G^>(t_1, t_2) = -\partial_{t_2} G^>(t_1, t_2) \Rightarrow G^>(t_1, t_2) = G^>(t_1 + dt, t_2 + dt)\,. \tag{4.4.7}$$

This is observed in our numerical solutions of the KB equations below. However, note that the instanteneously equilibrated configuration is not a thermal ensemble, so the final state cannot be a KM state.

Since, the initial theory is J_2 dominant(for step quench) or a $q = 2$ theory, we can start the quench from the corresponding ground state. We will present here only cases in which J_4 interaction is used to perform both step and bump quenches. We also found similar results for quenches using J_6 and J_8 interactions, as we expect from (4.4.7). The results are qualitatively similar for quenches starting from thermal state.

The value of the J_2 coupling is always fixed at 1. We will present results for step quench with initial $J_4 = 2$ which is suddenly turned off at time $t = 0$. For bump quench, we turn on $J_4 = 5$ for a time duration of $9 \times dt = 9 \times 0.05 = 0.45$ from time step $t = 1$ to $t = 10$. This same quench parameters are used for all quenches starting from different initial temperatures including the ones starting from ground state.

The step quench happens at $t = 0$, the two time arguments of $G^>(t-100, t)$ are outside the quench region if $t > 100$. The bump quench happens between $t = 0$ and $t = 11$ so the two time arguments are outside the quench region if $t \geq 111$. Figure (4.4) are plots of the real and imaginary parts of $G^>(t-100, t)$ as a function of time t for step and bump quenches starting from ground states. One can see that the Green's function freezes or equilibrates instantaneously once the two time arguments are outside the quench regions. But the equilibrated value is different from the thermal expectation value. Figure (4.5) compares $iG^K(\omega)/A(\omega)$ with $\tanh(\beta_f\omega/2)$ for step and bump quenches starting from initial inverse temperature $\beta = 10$.

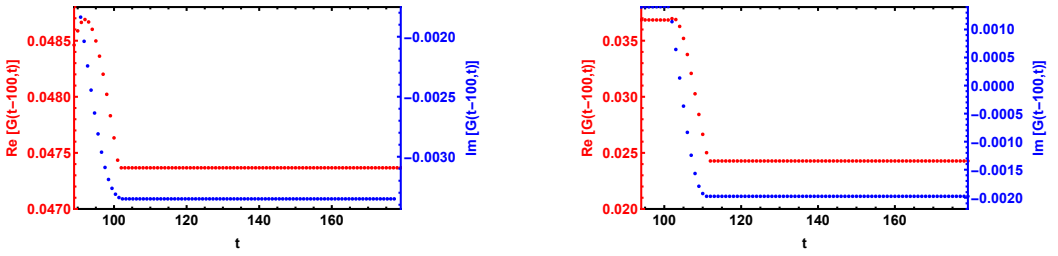

(a) Step quench at $t = 0$.

(b) Bump quench between $t = 1$ and $t = 10$

Figure 4.4: Plots of real and imaginary parts of $G^>(t-100, t)$ for (a) step quench, both the time arguments are outside the quench region for $t > 100$, and for (b) bump quench, both the time arguments are outside the quench region for $t \geq 111$. As we can see, the greater Green's function equilibrates instantaneously.

4.4.2 Quenches in $q = 4$ SYK model

In this subsection we will consider quantum quenches in which the final theory is $q = 4$ SYK model which only has 2-body (quartic, J_4) interaction. We will present results for which the interaction terms used for the quench process is J_2. We also found similar results for quenches with J_6 and J_8 interactions. For the initial thermal states, we considered three different inverse temperatures $\beta_i = 10$, 20, and 30. We find that increasing

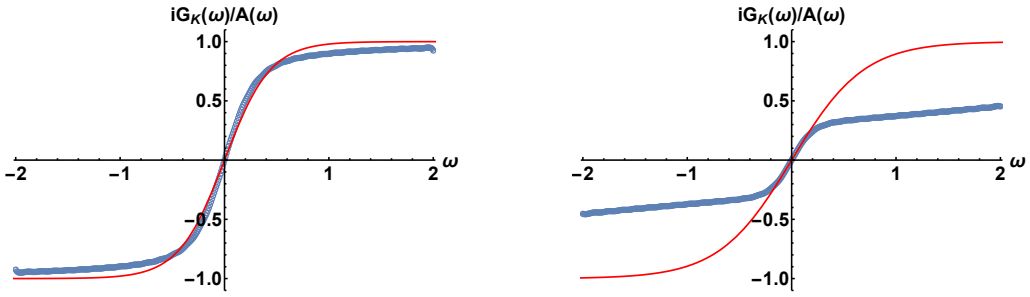

(a) Step quench, $\beta_i = 10$ (b) Bump quench, $\beta_i = 10$

Figure 4.5: Plots of $iG^K(\omega)/A(\omega)$ for the equilibrated limits of (a) step quench and (b) bump quench. For both the quenches, we start from a thermal state of inverse temperature $\beta_i = 10$. The red lines are plots for the function $\tanh(\beta\omega/2)$ with the respective β_f's.

the inverse temperature from 20 to 30 does not affect the results much. This is expected since for a fairly large β, the fermion distribution function is well represented by the step function (4.4.1). So, we expect that the quench starting from $\beta = 20$ and 30 should also be qualitatively similar and quantitatively close to the quenches starting from ground states.

Three different values of J_4 are used, namely, 0.5, 1 and 1.5. For step quenches, we start from a theory with J_4 and J_2. At $t = 0$, the J_2 coupling is suddenly changed to 0. For the bump quenches, starting from a theory with only J_4, J_2 is turned on for a time duration of $9 \times dt = 9 \times 0.05 = 0.45$ from time step $t = 1$ to $t = 10$. As mentioned above, we will use this time interval for all bump quench protocol. Changing this time interval does not affect our main results. Longer time interval only injects more energy into the system resulting in higher final temperature.

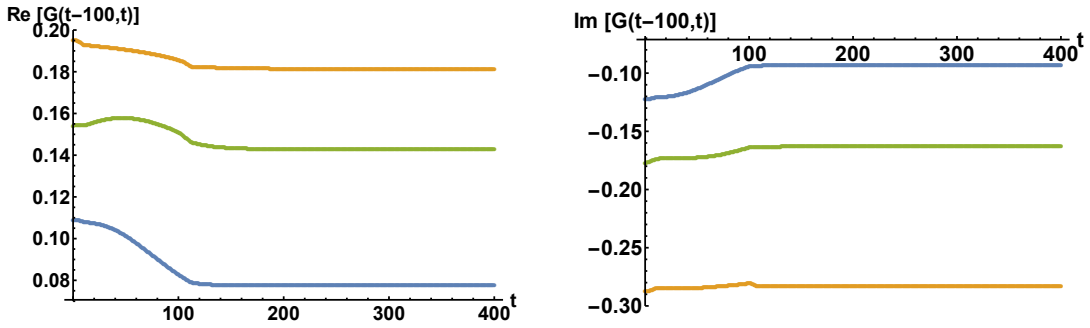

(a) (b)

Figure 4.6: (a) Real part of the greater Green's function $G^>(t-100, t)$ in the SYK model with quartic interaction and changing the quadratic interaction J_2 following bump protocol for three different set-up using different initial temperatures and different values of J_4 and J_2. (b) Imaginary part of the same greater Green's function $G^>(t-100, t)$.

Once both the time arguments are outside the quench region, we find that the greater Green's function thermalizes rapidly but not instantaneously, as can be seen in Figure(4.6). Figure (4.7a, 4.7b) are two resolved plots of $G^>(t-100, t)$ for different initial inverse temperatures as a function of t for step quenches. Since the step quench happens at $t = 0$, both the time arguments are outside the quench region if $t > 100$. Immediately after time

t crosses 100, $G^{>}(t-100,t)$ changes rapidly and exponentially towards its equilibrium thermal value. The evolutions for $t > 100$, both real and imaginary parts, fit exponential functions very well. The two exponents of the two exponential fits for real and imaginary parts are roughly equal. This behaviour is not a numerical artifact. The exponents do not change with change in time step size. We have checked for different time step sizes $dt = 0.05$ and $dt = 0.025$. Moreover, we have also checked energy conservation using (4.4.6).

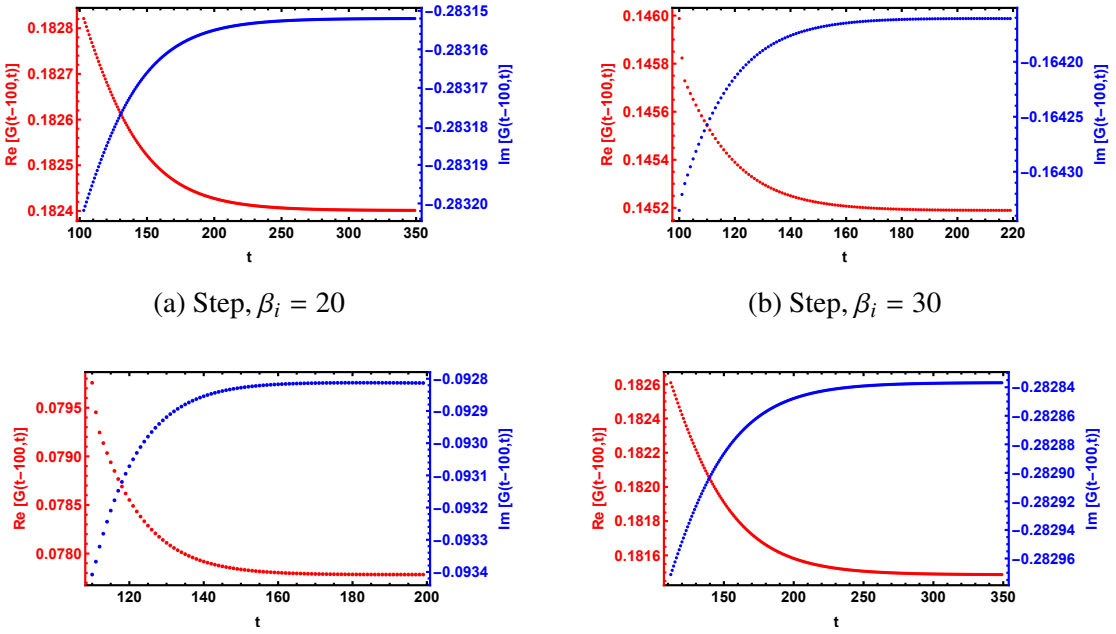

(a) Step, $\beta_i = 20$

(b) Step, $\beta_i = 30$

(c) Bump, $\beta_i = 10$

(d) Bump, $\beta_i = 20$

Figure 4.7: Real and imaginary parts of $G^{>}(t-100,t)$ for different quench protocols.

Similarly, for bump quenches in Figure (4.7c, 4.7d), once the two time arguments are outside the quench region, the Green's function thermalizes rapidly and its real and imaginary parts fit exponential functions very well. Below, we will consider only the exponent for the imaginary part which we will denote by γ_{Itt}.

$$Im[G^{>}(t-100,t)] \xrightarrow{\text{post quench region}} a_1 + b_1 e^{-\gamma_{Itt} t} \,. \tag{4.4.8}$$

The bump quench happens between time steps $t = 0$ and $t = 11$, so the two time arguments of $G^{>}(t-100,t)$ are outside the quench region if $t \geq 111$. One of the most interesting numerical result of this work is that we find that

$$\gamma_{Itt} = J_4 \,. \tag{4.4.9}$$

This can be seen from Fig. (4.8) and Table 4.1.

We also check if the final stationary limit is described by a thermal ensemble. For which we compare $iG^K(\omega)/A(\omega)$ with $\tanh(\beta_f \omega/2)$ for some final temperature β_f. Figure (4.9a, 4.9b) are two such comparisons. Figure (4.9a) is for step quench with $J_4 = 1$ and step profile of $J_2 = 0.03$ starting from initial temperature $\beta_i = 20$. Similarly, Figure (4.9b) is

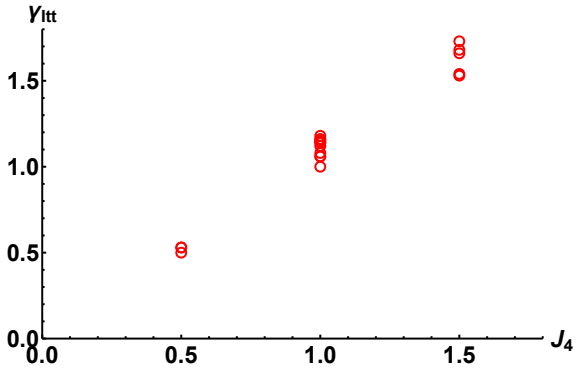

Figure 4.8: The exponent γ_{Itt} as a function of J_4.

for bump quench with $J_4 = 1$ and bump profile of $J_2 = 0.3$ from $t = 1$ to $t = 10$ starting from initial temperature $\beta_i = 20$. In all the other quenches, the stationary limit fits thermal ensemble very well as in these two examples.

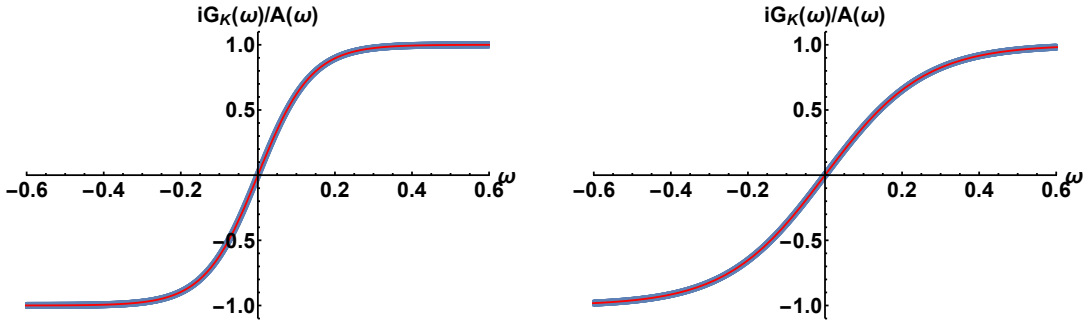

(a) Step quench, $\beta_i = 20, \beta_f = 14.53$ (b) Bump quench, $\beta_i = 20, \beta_f = 7.81$

Figure 4.9: Comparison of $iG^K(\omega)/A(\omega)$ (blue dots) with $\tanh(\beta_f\omega/2)$ (thin red line).

Since we observe thermalization, another observable of interest is $G^>(t, t_2)$ where t_2 is fixed. In the hydrodynamics limit [46] of large t, both the real and the imaginary parts of the expectation value of this observable are again exponential functions with both the exponents equal. We will consider the exponent of the imaginary part which we denote by γ_{It}. This exponent is equal to the exponent of the retarded Green's function in a thermal ensemble with temperature equal to the temperature of the final thermalized limit of the quench process. We will denote the exponent of the retarded Green's function by γ_{ret}.

$$Im[G^>(t,t_2)] \xrightarrow{t\to\infty} a_2 + b_2 e^{-\gamma_{It}t}, \qquad G^R(t,\beta_f) \xrightarrow{t\to\infty} a_3 + b_3 e^{-\gamma_{ret}t}\,. \tag{4.4.10}$$

At low temperature, γ_{It} is proportional to the final temperature.

$$\gamma_{It} = \gamma_{ret} \sim \frac{\pi}{2\beta_f}\,. \tag{4.4.11}$$

This result is similar to the result of [43] where after a change of variables from (t_1, t_2) to $(\mathcal{T} = t_1 + t_2, t = t_1 - t_2)$ and performing the Fourier transform with respect to t, one looks for the thermalization rate as a function of $\mathcal{T}$.

In a thermal ensemble, the retarded Green's function is a function of the relative time difference. In the conformal limit of SYK model, the retarded Green's function in a thermal ensemble of inverse temperature β is

$$\begin{aligned} G^R(t_1,t_2) = \quad & -i2b\cos(\pi\Delta)\left(\frac{\pi}{\sinh(2\pi(t_1-t_2)/\beta)}\right)^{\Delta}\theta(t_1-t_2) \\ & \xrightarrow{(t_1-t_2)\to\infty} -i2b\cos(\pi\Delta)(2\pi)^{\Delta}\, e^{-2\pi\Delta t/\beta}\,\theta(t_1-t_2)\,. \end{aligned} \tag{4.4.12}$$

where $\Delta = 1/q = 1/4$ and $b = (4\pi J_4^2)^{-1/4}$. In the conformal limit, the exponent is

$$\gamma_{conf} = \frac{2\pi\Delta}{\beta} = \frac{\pi}{2\beta}\,. \tag{4.4.13}$$

Figure (4.10) is the plot of γ_{It} and γ_{conf}.

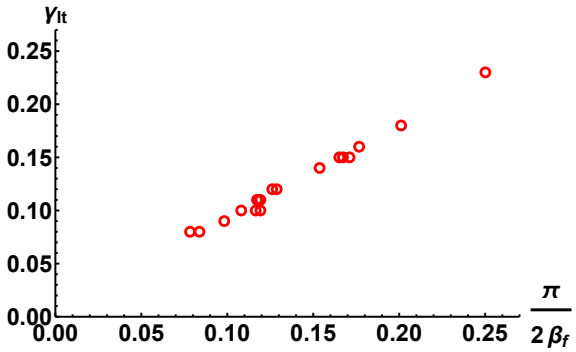

Figure 4.10: The exponent γ_{It} as a function of $\gamma_{conf} = \pi/(2\beta_f)$. $\gamma_{ret}x$ is exactly equal to γ_{It} as we can see from Table 4.1 so γ_{ret} is not plotted here.

At high temperatures, we find that the exponent of $G^R(t)$ gets significant correction compared to its value at the conformal limit. The corrected value of the exponent, which we have denoted by γ_{ret} above, is calculated by solving the SD equation numerically.

Important numerical results for the step and bump quenches with J_2, starting from different initial temperatures, are summarized in Table 4.1. We also calculate the exponent γ_{Itt} for $G^>(t, t-100)$, $G^>(t-300, t)$, $G^>(t, t-300)$, $G^>(t-500, t)$ and $G^>(t, t-500)$. The numerical values do not change significantly compared to the values given in Table 4.1 for $G^>(t-100, t)$ hence, we can conclude that $G^>(t-t_a, t)$ and $G^>(t, t-t_a)$ thermalize exponentially with the same exponent for arbitrary t_a.

Table 4.1: Numerical results for different quench protocols in $q = 4$ theory by changing J_2 coupling. The following are absolute values after taking care of the time step $dt = 0.05$. The value of J_4 is fixed during the entire quench process. The values of J_2 are the perturbations used to perform the different quench protocols.

J_4	Quench	J_2	β_i	β_f	γ_{Itt}	γ_{It}	γ_{ret}	γ_{conf}
0.5	Bump	0.1	20	18.75	0.50	0.08	0.08	0.08
0.5	"	0.3	20	13.17	0.53	0.10	0.10	0.12
0.5	Step	0.05	20	13.48	0.53	0.10	0.10	0.12
1.0	Bump	0.1	10	9.39	1.08	0.15	0.15	0.17
1.0	"	0.1	20	13.17	1.06	0.11	0.11	0.12
1.0	"	0.2	20	10.22	1.06	0.14	0.14	0.15
1.0	"	0.3	20	7.81	1.12	0.18	0.18	0.20
1.0	"	0.3	30	12.45	1.00	0.12	0.12	0.13
1.0	Step	0.03	10	9.51	1.16	0.15	0.15	0.17
1.0	"	0.03	20	14.53	1.16	0.10	0.10	0.11
1.0	"	0.04	10	9.18	1.14	0.15	0.15	0.17
1.0	"	0.04	20	13.32	1.15	0.11	0.11	0.12
1.0	"	0.05	20	12.20	1.14	0.12	0.12	0.13
1.0	"	0.05	30	13.39	1.18	0.11	0.11	0.12
1.5	Bump	0.1	10	8.89	1.68	0.16	0.16	0.18
1.5	"	0.1	20	15.99	1.54	0.09	0.09	0.10
1.5	"	0.1	30	20.05	1.53	0.08	0.08	0.08
1.5	"	0.3	10	5.31	1.73	0.26	0.26	0.30
1.5	"	0.3	20	6.28	1.66	0.23	0.23	0.25

5 Conclusion and Discussions

We divide this chapter in three sections which refer to the previous chapters and contains concluding remarks for each of the chapters.

5.1 Tuning of Chaos behavior

We have explored and demonstrated a tunable Lyapunov exponent by introducing conserved charges in the system, even when the charge is a simple U(1). We have considered SYK-type models, with complex fermions and a q-body all-to-all randomized interaction, in the $q \to \infty$ limit. For these models, we have explicitly demonstrated that a non-vanishing chemical potential has an exponentially large dominance over the q-body interaction coupling strength, in determining the chaos behaviour. It is expected, from the structure of the Schwinger-Dyson equations, that similar features hold for the tensor models [28], which share many interesting properties of the SYK-type interaction, but without the disorder averaging.

There are various interesting directions for future explorations. Given the results above, one may explore higher dimensional generalizations of the SYK-model, *e.g.* the model in [24], with an introduction of conserved charges. One would, naíively, expect a similar behaviour of the resulting Lyapunov exponent for the higher dimensional models; however, it would be very interesting to check how the details fall into the right places. Staying within the theme of a tuneable chaos, motivated by the similarities of SYK-model behaviour and random matrix behaviour at late times, it is natural to incorporate the effect of conserved charges in random matrix theories and analyze the consequences at late times [17].

From a holographic perspective, our analysis suggests that by introducing bulk gauge fields that correspond to introducing chemical potentials for the dual boundary theory, one should be able to do away with chaos completely, or, at least, should be able to tune down the Lyapunov exponent from its' maximal value. This would be an interesting aspect to check explicitly. Towards that, one presumably begins with a gravity description in *e.g.* $(d+1)$-dimensional bulk with AdS-asymptotic, and studies a scattering problem, *a la* [98], in the presence of a global charge. On a similar note, it is also very intriguing to explore the possibility of constructing an SYK-type model from explicit D-brane

construction in string theory, with or without global charges. One natural obstacle, for the SYK-type interaction, is to realize the dynamical origin of disorder averaging from the brane picture. Perhaps the large N tensor models can emerge more naturally in such scenarios. We are currently exploring some of these issues further.

5.2 Chaotic Correlation Function

We have computed the fermion six point function in the SYK model with complex fermions in the presence of a non-vanishing chemical potential. We then took triple short time limit of this correlation function so that it appears as a three point function of fermion bilinears. We show that the three point function of fermion bilinears, for $h \neq 2$ modes, have the scaling property of conformal field theory three point function, as is expected as a generalisation of the results of [48] to the complex fermion case. Like in [48], we find that the contribution of the contact three point graphs in the large q limit is subleading compared to that of the planar graphs.

We also compute three point function of fermion bilinears for the $h = 2$ mode. This mode is known to break the conformal invariance of the SYK model, both spontaneously as well as explicitly. This mode is known to exhibit chaotic behaviour with the Lyapunov exponent λ_{L} that saturates the chaos bound. The three point function of bilinears in this case has a behaviour different from those of the conformal, *i.e.*, $h \neq 2$ modes. In this case we find that in the large q limit, the contribution of the planar graphs is subleading compared to the contact graphs.

As a future direction to explore further, since the couplings of the SYK model are chosen from random gaussian distributions, it is tempting to ask if one can apply techniques of stochastic quantisation to reconstruct the bulk description. We hope to report on this soon.

5.3 Thermalization in SYK model

We studied quench in the SYK model with different quench protocols. While we have presented results for $q = 2$ theory, and $q = 4$ theory with step and bump quench protocols, we have carried out this analysis for $q = 6$ as well as for $q = 8$ models. We find that the qualitative features of the results are similar to the $q = 4$ cases.

We observed that the $q = 2$ theory does not thermalize for any of the quench scenario we considered. We considered quenching of J_4, J_6, and J_8 using step and bump protocol. The initial states that we considered are thermal states of inverse temperature $\beta_i = 10, 20,$ and 30 as well as the ground states. An interesting aspect of all the quenches is that the greater Green's function $G^{>}(t_1, t_2)$ equilibrates instantaneously as shown in (4.4.7). Its expectation value freezes once both the time arguments are outside the quench region. Although in the final states $G^{>}(t_1, t_2)$ equilibrates instantaneously, its equilibrium value is not the same as the thermal ensemble expectation value.

The instanteneous equilibation or freezing that we observed is like a glassy state. It can be shown that if the final theory have both J_2 and J_4 couplings, then two point functions always thermalize. This is true even for arbitrarily small J_4 coupling in the large N limit that we are considering. We expect that this would change if we consider effects subleading in N, where J_2 and J_4 couplings would truly start competing [22].

It would be interesting to identify the final state after each of these quenches. It is, however, beyond the scope of the present work since we are working only with the equations of motion of the $G^>(t_1, t_2)$ and solving them as an initial value problem. The $q = 2$ theory is not chaotic and does not satisfy the ETH, nevertheless thermalization in this theory is possible if the final state were a KM state (4.3.11). This, for example, happens quite often with step quenches in 1 + 1 dimensional theories (even in integrable theories) where the analog of KM states are the CC states (4.3.9).

In $q = 4$ theory, we find that thermalization happens in all the quench scenario we considered. We considered quenching with J_2, J_6, and J_8 using step and bump protocols. The initial states are thermal states of inverse temperature $\beta_i = 10, 20$, and 30. We examined two kinds of greater Green's functions, $G^>(t - t_a, t)$ and $G^>(t, t_b)$ as a function of time t with fixed t_a and t_b.

When both the time arguments $t - t_a$ and t are outside the quench region, both the real and imaginary parts of $G^>(t - t_a, t)$ are exponential functions with the same exponent. This exponent γ_{Itt} is equal to the value of coupling J_4 of the system.

The long time limit of both the real and imaginary parts of $G^>(t, t_b)$ are exponential functions with the same exponent. This exponent γ_{It} is equal to the exponent γ_{ret} of the retarded Green's function $G^R(t_1, t_2)$ in a thermal ensemble (4.4.12) with temperature equal to the final temperature of the quench process. This is obvious at least for the imaginary part of the $G^>(t, t_b)$ since the system thermalizes. $G^R(t_1, t_2)$ is a simple multiple of the imaginary part of $G^>(t_1, t_2)$. As one can see in Figure 5.1, the long time limit of $G^>(t, t_b)$ is calculated in a subset of the large $(t_1 - t_2)$ of $G^R(t_1, t_2)$.

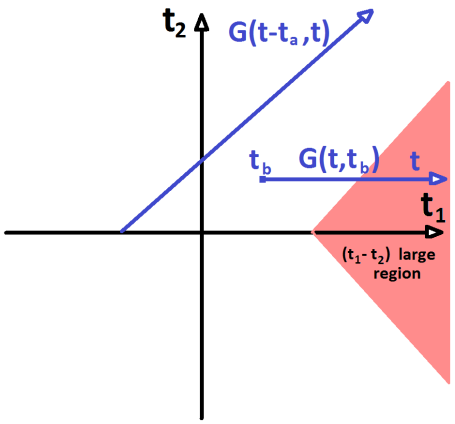

Figure 5.1: The large t limit of greater Green's function $G^>(t, t_b)$ is calculated in the large $(t_1 - t_2)$ region of the retarded Green's function $G^R(t_1, t_2)$. Moreover, in this region, the system has more or less thermalized. Hence, $\gamma_{It} = \gamma_{ret}$.

One clear and important observation that we can make is that the thermalization in $q = 4$ theory is not because the final state is a KM state. If the final state had been a KM state, $G^{>}(t - t_a, t)$ would have thermalized instantaneously once both its time arguments are outside the quench region.[1] This is because the 'diagonal' two-point function that we are considering are already thermalized in a KM state.

5.3.1 How to prepare KM states

The KM state, in principle, can be prepared by performing a *sudden* quantum quench starting from the ground state using the extra term

$$H_\mu(t) = i\mu(1 - \Theta(t)) \sum_{k=1}^{N/2} s_k \psi_k(t)\psi_{k+1}(t) \,, \tag{5.3.1}$$

where s_k's specifies the particular $|B_s\rangle$ defined in (4.3.10). This new term has been used in a different but related context in [90]. The argument behind this assertion is similar to the argument provided in [99] for the preparation of thermofield double state by performing a sudden quench. We will consider small μ limit. The full Hamiltonian before the quench at $t = 0$ is

$$H + H_\mu = (i)^{q/2} \sum_{1\le i_1<i_2<\ldots<i_q\le N} J_{i_1,i_2,\ldots,i_q}\psi_{i_1}\psi_{i_2}\ldots\psi_{i_q} + i\mu \sum_{k=1}^{N/2} s_k\psi_k(t)\psi_{k+1} \,. \tag{5.3.2}$$

The ground state of the above Hamiltonian is the state which minimizes the second term. But minimizing the second term corresponds to strong positive or negative correlation of ψ_k and ψ_{k+1} depending on the value of s_k. Strong correlation of ψ_k and ψ_{k+1} is the basis of the definition of $|B_s\rangle$ in (4.3.10). In hindsight, it is in some sense obvious why the KM states were not obtained from the step quench using the disordered couplings like $j_{2,ij}$ or J_2. This is because not just two fermions, but all the fermions were randomly and strongly correlated in the ground states of the initial Hamiltonians.

5.3.2 Ergodicity versus Mixing

In this work, we don't consider long time averaging. $q = 4$ theory satisfies eigenstate thermalization hypothesis(ETH). But thermalization from ETH crucially requires long time averaging. Thermalization without long time averaging has been observed in many other works but in most of the cases it is because the final state turns out to be a very particular state like CC states. So, in this sense, the thermalization that we observed is much more robust than what one expects from ETH. Thermalization with ETH follows from quantum ergodicity. But what we observe is more akin to a quantum version of mixing.

[1] Although quenches in $q = 4$ theory start from thermal states, as we have noted above the results should be qualitatively similar and quantitatively close to quenches starting from ground states.

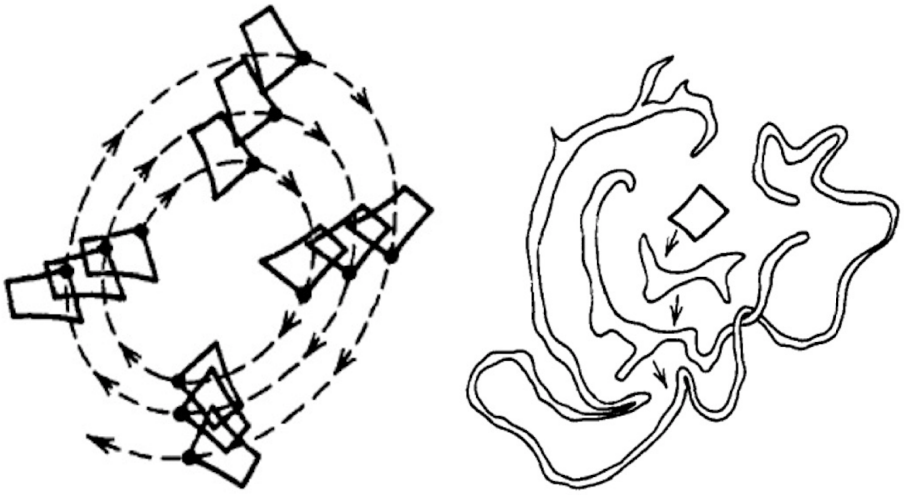

(a) Ergodicity (b) Mixing

Figure 5.2: (a) Ergodicity: the shape of the initial sample only changes slightly but sweeps out the entire allowed region under time evolution, (b) Mixing: the initial sample spreads out and reaches infinitesimally close to all the points in the allowed region of the phase space. Figure adopted from [85, 100].

In classical theories, mixing is a much stronger phenomenon compared to ergodicity. Figure (5.2a) shows ergodic evolution in the classical phase space. The initial state is described by an ensemble concentrated in the deformed rectangle in the phase space. The volume is conserved under time evolution due to the Liouville theorem for a closed system, but the shape can change. For ergodic systems, the shape of the initial sample hardly changes but it sweeps out the entire allowed space under time evolution. So, a long time averaging gives the expectation value in the micro-canonical ensemble. In mixing, as shown in Figure (5.2b), the initial sample spreads out and reaches infinitesimally close to all the points in the allowed region of the phase space. So, without time averaging, mixing gives the expectation value in the microcanonical ensemble.

Using this classical analogy, we believe that even in quantum systems, chaos is a much stronger condition for thermalization than the eigenstate thermalization hypothesis(ETH). Our results on thermalization in the quenched SYK model seem to suggest that quench without long time average is a quantum analog of mixing. It would be interesting to make this more concrete. We hope to return to this soon.

Bibliography

[1] G. Casati, *CHAOS IN QUANTUM MECHANICS*, .

[2] A. Peres, *Ergodicity and mixing in quantum theory. I*, *Phys. Rev.* **A30** (1984) 504–508.

[3] D. R. Grempel, R. E. Prange, and S. Fishman, *Quantum dynamics of a nonintegrable system*, *Phys. Rev.* **A29** (1984) 1639–1647.

[4] A. Peres, *New Conserved Quantities and Test for Quantum Chaos*, *Phys. Rev. Lett.* **53** (1984) 1711.

[5] G. Casati and I. Guarneri, *Chaos and Spectral Features of Quantum Systems Under External Perturbations*, *Phys. Rev. Lett.* **50** (1983) 640.

[6] J. Cotler and N. Hunter-Jones, *Spectral decoupling in many-body quantum chaos*, arXiv:1911.02026 [hep-th].

[7] I. Rivin, *Random Graphs from Random Matrices*, arXiv:1910.08253 [math.PR].

[8] D. Stanford and E. Witten, *JT Gravity and the Ensembles of Random Matrix Theory*, arXiv:1907.03363 [hep-th].

[9] M. A. Nowak and W. Tarnowski, *Narain transform for spectral deformations of random matrix models*, arXiv:1909.05759 [math-ph].

[10] A. B. Jaiswal, A. Pandey, and R. Prakash, *Universality classes of quantum chaotic dissipative systems*, *EPL* **127** no. 3, (2019) 30004.

[11] J. Maldacena, S. H. Shenker, and D. Stanford, *A bound on chaos*, *JHEP* **08** (2016) 106, arXiv:1503.01409 [hep-th].

[12] S. Ray, S. Sinha, and K. Sengupta, *Signature of chaos and delocalization in a periodically driven many-body system: An out-of-time-order-correlation study*, *Phys. Rev.* **A98** no. 5, (2018) 053631, arXiv:1804.01545 [cond-mat.quant-gas].

[13] C.-J. Lin and O. I. Motrunich, *Out-of-time-ordered correlators in a quantum Ising chain*, *Phys. Rev.* **B97** no. 14, (2018) 144304, arXiv:1801.01636 [cond-mat.stat-mech].

[14] M. Blake, H. Lee, and H. Liu, *A quantum hydrodynamical description for scrambling and many-body chaos*, *JHEP* **10** (2018) 127, arXiv:1801.00010 [hep-th].

[15] Y. Sekino and L. Susskind, *Fast Scramblers*, *JHEP* **10** (2008) 065, arXiv:0808.2096 [hep-th].

[16] S. H. Shenker and D. Stanford, *Black holes and the butterfly effect*, *JHEP* **03** (2014) 067, arXiv:1306.0622 [hep-th].

[17] J. S. Cotler, G. Gur-Ari, M. Hanada, J. Polchinski, P. Saad, S. H. Shenker, D. Stanford, A. Streicher, and M. Tezuka.

[18] A. Jevicki, K. Suzuki, and J. Yoon, *Bi-local holography in the syk model*, *JHEP* **07** (2016) 007, arXiv:1603.06246 [hep-th].

[19] I. Danshita, M. Hanada, and M. Tezuka, *Creating and probing the Sachdev-Ye-Kitaev model with ultracold gases: Towards experimental studies of quantum gravity*, *PTEP* **2017** no. 8, (2017) 083I01, arXiv:1606.02454 [cond-mat.quant-gas].

[20] J. Sonner and M. Vielma, *Eigenstate thermalization in the Sachdev-Ye-Kitaev model*, *JHEP* **11** (2017) 149, arXiv:1707.08013 [hep-th].

[21] J. Maldacena and D. Stanford, *Remarks on the Sachdev-Ye-Kitaev model*, *Phys. Rev.* **D94** no. 10, (2016) 106002, arXiv:1604.07818 [hep-th].

[22] A. M. García-García, B. Loureiro, A. Romero-Bermúdez, and M. Tezuka, *Chaotic-integrable transition in the sachdev-ye-kitaev model*, *Phys. Rev. Lett.* **120** (Jun, 2018) 241603. https://link.aps.org/doi/10.1103/PhysRevLett.120.241603.

[23] P. Narayan and J. Yoon, *SYK-like Tensor Models on the Lattice*, *JHEP* **08** (2017) 083, arXiv:1705.01554 [hep-th].

[24] G. Turiaci and H. Verlinde, *Towards a 2d QFT Analog of the SYK Model*, *JHEP* **10** (2017) 167, arXiv:1701.00528 [hep-th].

[25] D. J. Gross and V. Rosenhaus, *A Generalization of Sachdev-Ye-Kitaev*, *JHEP* **02** (2017) 093, arXiv:1610.01569 [hep-th].

[26] W. Fu, D. Gaiotto, J. Maldacena, and S. Sachdev, *Supersymmetric sachdev-ye-kitaev models*, *Phys. Rev.* **D95** no. 2, (2017) 026009, arXiv:1610.08917 [hep-th]. [Addendum: Phys. Rev.D95,no.6,069904(2017)].

[27] P. Narayan and J. Yoon, *Supersymmetric SYK Model with Global Symmetry*, *JHEP* **08** (2018) 159, arXiv:1712.02647 [hep-th].

[28] E. Witten, *An SYK-Like Model Without Disorder*, arXiv:1610.09758 [hep-th].

[29] I. R. Klebanov and G. Tarnopolsky, *Uncolored random tensors, melon diagrams, and the Sachdev-Ye-Kitaev models*, *Phys. Rev.* **D95** no. 4, (2017) 046004, arXiv:1611.08915 [hep-th].

[30] K. Bulycheva, I. R. Klebanov, A. Milekhin, and G. Tarnopolsky, *Spectra of Operators in Large N Tensor Models*, *Phys. Rev.* **D97** no. 2, (2018) 026016, arXiv:1707.09347 [hep-th].

[31] I. R. Klebanov, F. Popov, and G. Tarnopolsky, *TASI Lectures on Large N Tensor Models*, *PoS* **TASI2017** (2018) 004, arXiv:1808.09434 [hep-th].

[32] S. Choudhury, A. Dey, I. Halder, L. Janagal, S. Minwalla, and R. Poojary, *Notes on melonic $O(N)^{q-1}$ tensor models*, *JHEP* **06** (2018) 094, arXiv:1707.09352 [hep-th].

[33] C. Krishnan, S. Sanyal, and P. N. Bala Subramanian, *Quantum Chaos and Holographic Tensor Models*, *JHEP* **03** (2017) 056, arXiv:1612.06330 [hep-th].

[34] C. Krishnan, K. V. Pavan Kumar, and D. Rosa, *Contrasting SYK-like Models*, *JHEP* **01** (2018) 064, arXiv:1709.06498 [hep-th].

[35] T. Nishinaka and S. Terashima, *A note on SachdevâĂŞYeâĂŞKitaev like model without random coupling*, *Nucl. Phys.* **B926** (2018) 321–334, arXiv:1611.10290 [hep-th].

[36] R. A. Davison, W. Fu, A. Georges, Y. Gu, K. Jensen, and S. Sachdev, *Thermoelectric transport in disordered metals without quasiparticles: The Sachdev-Ye-Kitaev models and holography*, *Phys. Rev.* **B95** no. 15, (2017) 155131, arXiv:1612.00849 [cond-mat.str-el].

[37] S. Banerjee and E. Altman, *Solvable model for a dynamical quantum phase transition from fast to slow scrambling*, *Phys. Rev.* **B95** no. 13, (2017) 134302, arXiv:1610.04619 [cond-mat.str-el].

[38] C. Krishnan and K. V. P. Kumar, *Towards a Finite-N Hologram*, *JHEP* **10** (2017) 099, arXiv:1706.05364 [hep-th].

[39] S. H. Strogatz, *Nonlinear Dynamics and Chaos*. Addison Wesley, Reading, MA, 1994.

[40] S. Chaudhuri and R. Loganayagam, *Probing out-of-time-order correlators*, *JHEP* **07** (2019) 006, arXiv:1807.09731 [hep-th].

[41] B. Chakrabarty, S. Chaudhuri, and R. Loganayagam, *Out of time ordered quantum dissipation*, *JHEP* **07** (2019) 102, arXiv:1811.01513 [cond-mat.stat-mech].

[42] S. Chaudhuri, C. Chowdhury, and R. Loganayagam, *Spectral representation of thermal oto correlators*, *JHEP* **02** (2019) 018, arXiv:1810.03118 [hep-th].

[43] A. Eberlein, V. Kasper, S. Sachdev, and J. Steinberg, *Quantum quench of the Sachdev-Ye-Kitaev Model*, *Phys. Rev.* **B96** no. 20, (2017) 205123, arXiv:1706.07803 [cond-mat.str-el].

[44] D. Das, S. R. Das, D. A. Galante, R. C. Myers, and K. Sengupta, *An exactly solvable quench protocol for integrable spin models*, *JHEP* **11** (2017) 157, arXiv:1706.02322 [hep-th].

[45] G. Mandal, S. Paranjape, and N. Sorokhaibam, *Thermalization in 2D critical quench and UV/IR mixing*, *JHEP* **01** (2018) 027, arXiv:1512.02187 [hep-th].

[46] S. Bhattacharyya and S. Minwalla, *Weak Field Black Hole Formation in Asymptotically AdS Spacetimes*, *JHEP* **09** (2009) 034, arXiv:0904.0464 [hep-th].

[47] E. Caceres, A. Kundu, J. F. Pedraza, and D.-L. Yang, *Weak Field Collapse in AdS: Introducing a Charge Density*, *JHEP* **06** (2015) 111, arXiv:1411.1744 [hep-th].

[48] D. J. Gross and V. Rosenhaus, *The Bulk Dual of SYK: Cubic Couplings*, *JHEP* **05** (2017) 092, arXiv:1702.08016 [hep-th].

[49] D. J. Gross and V. Rosenhaus, *All point correlation functions in SYK*, *JHEP* **12** (2017) 148, arXiv:1710.08113 [hep-th].

[50] A. Y. Kitaev, *Entanglement in strongly-correlated quantum matter*, . Talk at KITP, University of California, Santa Barbara.

[51] J. Engelsöy, T. G. Mertens, and H. Verlinde, *An investigation of AdS_2 backreaction and holography*, *JHEP* **07** (2016) 139, arXiv:1606.03438 [hep-th].

[52] K. Jensen, *Chaos in AdS_2 Holography*, *Phys. Rev. Lett.* **117** no. 11, (2016) 111601, arXiv:1605.06098 [hep-th].

[53] J. Maldacena, D. Stanford, and Z. Yang, *Conformal symmetry and its breaking in two dimensional Nearly Anti-de-Sitter space*, *PTEP* **2016** no. 12, (2016) 12C104, arXiv:1606.01857 [hep-th].

[54] A. Kitaev and S. J. Suh, *The soft mode in the Sachdev-Ye-Kitaev model and its gravity dual*, *JHEP* **05** (2018) 183, arXiv:1711.08467 [hep-th].

[55] S. R. Das, A. Jevicki, and K. Suzuki, *Three Dimensional View of the SYK/AdS Duality*, *JHEP* **09** (2017) 017, arXiv:1704.07208 [hep-th].

[56] J. Polchinski and V. Rosenhaus, *The spectrum in the sachdev-ye-kitaev model*, *JHEP* **04** (2016) 001, arXiv:1601.06768 [hep-th].

[57] N. Callebaut and H. Verlinde, *Entanglement Dynamics in 2D CFT with Boundary: Entropic origin of JT gravity and Schwarzian QM*, arXiv:1808.05583 [hep-th].

[58] A. Gaikwad, L. K. Joshi, G. Mandal, and S. R. Wadia, *Holographic dual to charged SYK from 3D Gravity and Chern-Simons*, arXiv:1802.07746 [hep-th].

[59] D. Stanford and E. Witten, *Fermionic Localization of the Schwarzian Theory*, *JHEP* **10** (2017) 008, arXiv:1703.04612 [hep-th].

[60] M. Babadi, E. Demler, and M. Knap, *Far-from-equilibrium field theory of many-body quantum spin systems: Prethermalization and relaxation of spin spiral states in three dimensions*, *Phys. Rev. X* **5** (Oct, 2015) 041005. https://link.aps.org/doi/10.1103/PhysRevX.5.041005.

[61] K. Bulycheva, *A note on the SYK model with complex fermions*, *JHEP* **12** (2017) 069, arXiv:1706.07411 [hep-th].

[62] P. Basu and K. Jaswin, *Higher point otocs and the bound on chaos*, arXiv:1809.05331 [hep-th].

[63] C. Gogolin and J. Eisert, *Equilibration, thermalisation, and the emergence of statistical mechanics in closed quantum systems*, *Rept. Prog. Phys.* **79** no. 5, (2016) 056001, arXiv:1503.07538 [quant-ph].

[64] J. H. Traschen and R. H. Brandenberger, *Particle Production During Out-of-equilibrium Phase Transitions*, *Phys. Rev.* **D42** (1990) 2491–2504.

[65] M. Cramer, C. M. Dawson, J. Eisert, and T. J. Osborne, *Exact relaxation in a class of nonequilibrium quantum lattice systems*, *Phys. Rev. Lett.* **100** (Jan, 2008) 030602. https://link.aps.org/doi/10.1103/PhysRevLett.100.030602.

[66] J. Erdmenger, M. Flory, M.-N. Newrzella, M. Strydom, and J. M. S. Wu, *Quantum Quenches in a Holographic Kondo Model*, *JHEP* **04** (2017) 045, arXiv:1612.06860 [hep-th].

[67] J. Cardy, *Thermalization and Revivals after a Quantum Quench in Conformal Field Theory*, *Phys. Rev. Lett.* **112** (2014) 220401, arXiv:1403.3040 [cond-mat.stat-mech].

[68] A. Polkovnikov, K. Sengupta, A. Silva, and M. Vengalattore, *Nonequilibrium dynamics of closed interacting quantum systems*, *Rev. Mod. Phys.* **83** (2011) 863, arXiv:1007.5331 [cond-mat.stat-mech].

[69] P. Calabrese and J. Cardy, *Quantum Quenches in Extended Systems*, *J. Stat. Mech.* **0706** (2007) P06008, arXiv:0704.1880 [cond-mat.stat-mech].

[70] M. Haque and P. McClarty, *Eigenstate Thermalization Scaling in Majorana Clusters: from Integrable to Chaotic SYK Models*, arXiv:1711.02360 [cond-mat.stat-mech].

[71] G. Mandal, R. Sinha, and N. Sorokhaibam, *Thermalization with chemical potentials, and higher spin black holes*, *JHEP* **08** (2015) 013, arXiv:1501.04580 [hep-th].

[72] S. R. Das, D. A. Galante, and R. C. Myers, *Smooth and fast versus instantaneous quenches in quantum field theory*, *JHEP* **08** (2015) 073, arXiv:1505.05224 [hep-th].

[73] A. Goel, H. T. Lam, G. J. Turiaci, and H. Verlinde, *Expanding the Black Hole Interior: Partially Entangled Thermal States in SYK*, arXiv:1807.03916 [hep-th].

[74] N. Hunter-Jones, J. Liu, and Y. Zhou, *On thermalization in the SYK and supersymmetric SYK models*, *JHEP* **02** (2018) 142, arXiv:1710.03012 [hep-th].

[75] T. Anous, T. Hartman, A. Rovai, and J. Sonner, *Black Hole Collapse in the 1/c Expansion*, *JHEP* **07** (2016) 123, arXiv:1603.04856 [hep-th].

[76] T. Anous, T. Hartman, A. Rovai, and J. Sonner, *From Conformal Blocks to Path Integrals in the Vaidya Geometry*, *JHEP* **09** (2017) 009, arXiv:1706.02668 [hep-th].

[77] T. Hartman and J. Maldacena, *Time Evolution of Entanglement Entropy from Black Hole Interiors*, *JHEP* **05** (2013) 014, arXiv:1303.1080 [hep-th].

[78] A. Mollabashi, M. Nozaki, S. Ryu, and T. Takayanagi, *Holographic Geometry of cMERA for Quantum Quenches and Finite Temperature*, *JHEP* **03** (2014) 098, arXiv:1311.6095 [hep-th].

[79] M. Nozaki, S. Ryu, and T. Takayanagi, *Holographic Geometry of Entanglement Renormalization in Quantum Field Theories*, *JHEP* **10** (2012) 193, arXiv:1208.3469 [hep-th].

[80] D.-W. Pang, *Holographic entanglement entropy of nonlocal field theories*, *Phys. Rev.* **D89** no. 12, (2014) 126005, arXiv:1404.5419 [hep-th].

[81] J. M. Deutsch, *Quantum statistical mechanics in a closed system*, *Phys. Rev. A* **43** (Feb, 1991) 2046–2049. https://link.aps.org/doi/10.1103/PhysRevA.43.2046.

[82] M. Srednicki, *Entropy and area*, *Phys. Rev. Lett.* **71** (1993) 666–669, arXiv:hep-th/9303048 [hep-th].

[83] D. Fioretto and G. Mussardo, *Quantum quenches in integrable field theories*, *New Journal of Physics* **12** no. 5, (2010) 055015.

[84] P. Calabrese and J. L. Cardy, *Time-dependence of correlation functions following a quantum quench*, *Phys. Rev. Lett.* **96** (2006) 136801, arXiv:cond-mat/0601225 [cond-mat].

[85] S. Ziraldo *et al.*, *Thermalization and relaxation after a quantum quench in disordered Hamiltonians*. PhD thesis, SISSA, 2013.

[86] P. Calabrese and J. Cardy, *Quantum quenches in 1+1 dimensional conformal field theories*, *J. Stat. Mech.* **1606** no. 6, (2016) 064003, arXiv:1603.02889 [cond-mat.stat-mech].

[87] M. Greiner, O. Mandel, T. W. Hänsch, and I. Bloch, *Collapse and revival of the matter wave field of a bose–einstein condensate*, *Nature* **419** no. 6902, (2002) 51.

[88] T. Kinoshita, T. Wenger, and D. S. Weiss, *A quantum newton's cradle*, *Nature* **440** no. 7086, (2006) 900.

[89] P. Calabrese and J. L. Cardy, *Evolution of entanglement entropy in one-dimensional systems*, *J. Stat. Mech.* **0504** (2005) P04010, arXiv:cond-mat/0503393 [cond-mat].

[90] I. Kourkoulou and J. Maldacena, *Pure states in the SYK model and nearly-AdS_2 gravity*, arXiv:1707.02325 [hep-th].

[91] J. Maciejko, *An introduction to nonequilibrium many-body theory*. Springer, 2007.

[92] J. M. Magan, *Random free fermions: An analytical example of eigenstate thermalization*, *Phys. Rev. Lett.* **116** no. 3, (2016) 030401, arXiv:1508.05339 [quant-ph].

[93] M. Rigol and M. Srednicki, *Alternatives to eigenstate thermalization*, *Phys. Rev. Lett.* **108** (Mar, 2012) 110601. https://link.aps.org/doi/10.1103/PhysRevLett.108.110601.

[94] V. Balasubramanian, A. Bernamonti, J. de Boer, N. Copland, B. Craps, E. Keski-Vakkuri, B. Muller, A. Schafer, M. Shigemori, and W. Staessens, *Holographic Thermalization*, *Phys. Rev.* **D84** (2011) 026010, arXiv:1103.2683 [hep-th].

[95] J. Cardy, *Bulk Renormalization Group Flows and Boundary States in Conformal Field Theories*, *SciPost Phys.* **3** no. 2, (2017) 011, arXiv:1706.01568 [hep-th].

[96] S. Paranjape and N. Sorokhaibam, *Exact Growth of Entanglement and Dynamical Phase Transition in Global Fermionic Quench*, arXiv:1609.02926 [hep-th].

[97] A. Kamenev, *Field theory of non-equilibrium systems*. Cambridge University Press, 2011.

[98] S. H. Shenker and D. Stanford, *Stringy effects in scrambling*, *JHEP* **05** (2015) 132, arXiv:1412.6087 [hep-th].

[99] J. Maldacena and X.-L. Qi, *Eternal traversable wormhole*, arXiv:1804.00491 [hep-th].

[100] R. Balescu, *Equilibrium and nonequilibrium statistical mechanics*. New York, NY: Wiley, 1975.